1   **Fingerprints of a New Normal Urban Air Quality in the United States**

2   S. Kondragunta[*1], Z. Wei[2], B. C. McDonald[3], D. L. Goldberg[4], D. Q. Tong[5]

3   [1]NOAA NESDIS Center for Satellite Applications and Research, 5825 University Research
4   Court, College Park, MD

5   [2]IM Systems Group, 5825 University Research Court, College Park, MD

6   [3]NOAA Chemical Systems Laboratory, Boulder, CO

7   [4]Milken School of Public Health, George Washington University, Washington, DC

8   [5]Department of Atmospheric, Oceanic, and Earth Sciences, George Mason University, Fairfax,
9   VA

10

11

12

13

14

15

16

17

18

19

20

21

22

23

24

25

26

27

28

[*] Corresponding author: Phone: 301-655-7311. Email: Shobha.Kondragunta@noaa.gov

29

Abstract

31   Most countries around the world including the United States took actions to control

32   COVID-19 spread that included social distancing, limiting air and ground travel, closing schools,

33   suspending sports leagues, closing factories etc., leading to an abrupt shift in human activity. On-

34   road NO_x emissions from light and heavy duty vehicles decreased by 9% to 19% between

35   February and March at the onset of lockdown in the middle of March in most of the US; between

36   March and April, the on-road NO_x emissions dropped further by 8% to 31% when lockdown

37   measures were the most stringent. These precipitous drops in NO_x emissions correlated well

38   with tropospheric NO_2 column amount observed by Sentinel 5 Precursor TROPOspheric

39   Monitoring Instrument (S5P TROPOMI). Further, the changes in TROPOMI tropospheric NO_2

40   across the continental U.S. between 2020 and 2019 correlated well with changes in on-road NO_x

41   emissions (r = 0.68) but correlated weakly with changes in emissions from the power plants (r =

42   0.35). These findings confirm the known knowledge that power plants are no longer a major

43   source of NO_2 in urban areas of the US. With increased unemployment rate in 2020 after the

44   lockdown combined with telework policies across the nation for non-essential workers, the NO_2

45   values decreased at the rate of 0.8 $\mu moles/m^2$ decrease per unit percentage increase in

46   unemployment rate. Across the urban regions we found positive correlation between S5P

47   TROPOMI NO_2 and Suomi NPP Visible Infrared Imaging Radiometer Suite (VIIRS) aerosol

48   optical depths indicating common source sectors for NO_2 and aerosols/aerosol precursors.

49   **Key Words:** COVID-19, nitrogen dioxide, aerosol optical depth, TROPOMI, NOx emissions

50

Plain Language Summary

52   This study documents the different phases of lockdown and how traffic emissions

53   changed accordingly across the US and in particular in five different cities, namely Los Angeles,

54   San Francisco, San Joaquin Valley, New York City, and Atlanta. Analysis of data for these

55   cities from measurements on the ground and satellite data indicate that a down turn in economy

56   and telework policies reduced the number of cars and trucks on the road in March and April due

57   to which air quality got better. This provided a window into the future as to how we can achieve

58   improved air quality.

59

60

61

62

63

64

65

66

67

68

69

70

71

72

73

74   ## 1. Introduction

75   As the 2019 novel Corona virus (COVID-19) spread from China to other parts of the world,

76   various countries imposed lockdown measures one by one. Reports of improved air quality from

77   ground and satellite observations of aerosol optical depth and nitrogen dioxide soon followed in

78   the media as documented by Kondragunta et al. (2020). The precipitous drops seen in the

79   tropospheric vertical column nitrogen dioxide (NO_2, $tropNO_2$ here onwards) measured by the

80   Sentinel 5P Tropospheric Monitoring Instrument (TROPOMI) were substantial, especially

81   during the strict lockdown period for each country (Gkatzelis et al., 2020). Goldberg et al.

82   (2020) reported that in the United States (US), $tropNO_2$ decreased by 9.2% to 45% in 26 cities

83   during March 15 to April 30, 2020 compared to the same time period in 2019; these reported

84   reductions account for the influence of the weather. Other researchers reported similar findings,

85   mainly reductions of $tropNO_2$ attributed to reductions in traffic emissions both in the U.S. and

86   across the globe in major urban areas of Europe, India, and China (Bauwens et al., 2020; Keller

87   et al., 2020; Zheng et al., 2020; Vaderu et al., 2020; Straka et al., 2020; Nager et al., 2020). For

88   example in Washington D.C., average distance traveled by people dropped by 60% between

89   February and April when restrictions were fully in place (Straka et al., 2020). This sudden drop

90   in tropNO2 in major metropolitan areas where transportation source sector for NO_x is strong is

91   due to reduced traffic on top of an already observed general decreasing trend in NO_x emissions.

92   According to Lamsal et al. (2015), $tropNO_2$ observed by the Ozone Monitoring Instrument

93   showed a decreasing trend with an overall decrease of 28% between 2005 and 2013. These

94   reductions are consistent with NO_x emissions reductions from major power plants in the US due

95   to Clean Air Interstate Rule and Cross State Air Pollution Rule. The NO_x emissions continued to

96   drop as more and more power plants switched to natural gas or began to rely on clean coal (de

97   Gouw et al., 2014)

98   The significance of NO_2 is that it is a precursor for both ozone and particulate matter,

99   primary components of photochemical smog. Whether it enhances or decreases ozone

100   production is dependent on a given region being NO_x saturated or volatile organic compound

101   (VOC) saturated, the inherent non-linearity of ozone photochemistry (Kroll et al., 2020;

102   Mazzuca et al., 2016). The two main sources of NO_2 in the US are energy sector and

103   transportation sector according to the 2014 Community Emissions Data System (Hoesly et al.,

104   2018).   A study by Zheng et al. (2020) analyzed the reductions in trace gas and aerosol

105   concentrations in China during the lockdown and found that the most significant drop in aerosols

106   was for nitrate aerosol. For the time period corresponding to the lockdown in China, January 23

107   to February 22, 2020, mean nitrate aerosol concentration was 14.1 $\mu g/m^3$; for the same time

108   period in 2019, concentration was 23.8 $\mu g/m^3$. This 41% reduction is corroborated by reductions

109   in NO_2 observed by TROPOMI (Bauwens et al., 2020).

110   Though NO_2 is considered important due to its ozone and aerosol producing potential, it has

111   harmful human health impacts when inhaled. Achakulwisut et al (2019) showed that 64% of four

112   million pediatric asthma cases each year are due to exposure to NO_2. It should be noted though

113   that NO_2 was used as a proxy for traffic-related pollution. The World Health Organization

114   (WHO) standard for NO_2 is an annual average of 21 parts per billion and for the US, it is 53 parts

115   per billion.   The authors do note that that daily exposures to NO_2 can vary from annual averages

116   and traffic pollution is usually a mixture of precursor gases, primary particulates, and

117   photochemically formed ozone and aerosols. Nevertheless, when countries went into lockdown,

118   the most noticeable indication of a drop in traffic related pollution is $tropNO_2$ in urban areas

119   observed by TROPOMI, lending support to the assumption that NO_2 is a good proxy for traffic

120   related pollution.   The COVID-19 lockdown measures disproportionately impacted traffic more

121   than industrial operations. We analyzed TROPOMI $tropNO_2$ and Suomi National Polar-orbiting

122   Partnership Visible Infrared Imaging Radiometer Suite (Suomi NPP VIIRS) AOD data in

123   conjunction with on-road NO_x ($NO+NO_2$) emissions data, NO_x emissions from power plants, and

124   unemployment rates where available. The goal of this study is to examine the trends in on-road

125   and power plant emissions for five different locations (four urban areas and one rural area) to

126   answer the questions: (1) are changes in NO_x emissions during the lockdown detectable in

127   TROPOMI tropNO_2 data, (2) are the economic indicators consistent with emissions changes, and

128   (3) are the trends reversing with the removal of lockdown measures in the major metro areas.

129   These questions are answered with spatial and temporal analysis of ground-based observations

130   and satellite data, relating indicators of human activity during and prior to COVID-19 lockdown

131   with air quality, and examining if a new normal urban air quality can be achieved with novel

132   policies.

2. Methods

2.1.   Sentinel 5P TROPOMI NO2

134
135

136   The TROPOMI NO_2 algorithm is based on the Differential Optical Absorption

137   Spectroscopy technique that involves fitting the spectra in the NO_2 absorption region between

138   405 nm and 465 nm using known laboratory-measured reference absorption spectra. The

139   Sentinel 5P flies in formation with SNPP. Though some Sentinel 5P trace gas algorithm

140   retrievals depend on VIIRS cloud mask, the NO_2 algorithm relies on cloud retrievals using its

141   oxygen A-band absorption (van Geffen et al., 2019). The cloud fraction and cloud top pressure

142   are used in air mass factor calculation for partially cloudy pixels. There is an indication that the

143   cloud algorithm is likely conservatively masking out good NO_2 retrievals according to a

144   validation study conducted by Judd et al. (2020). Though Judd et al (2020) used data with

145   quality flag equals to unity, we used the quality flag value recommended by the NO_2 algorithm

146   theoretical basis document (van Geffen et al., 2019). Only data with quality flag > 0.75 were

147   used as this quality flag setting ensures that cloudy retrievals or retrievals with snow/ice covered

148   pixels are screened out. The TROPOMI Level 2 product file consists of pixel level (3.5 km x 5.6

149   km) NO_2 column amount for troposphere that we used in this study. The NO_2 algorithm

150   retrieves total column NO_2 and separates the stratosphere from troposphere using chemical

151   transport model predicted stratospheric NO_2 analysis fields (van Geffen et al., 2019). The

152   expected accuracy of tropospheric NO_2 column for polluted regions with high NO_2 values is

153   ~25% and independent validation efforts using ground based spectrometers such as Pandora have

154   confirmed that tropNO2 is generally under estimated, especially in polluted regions and that

155   significant sources of errors come from coarser resolution a priori profiles used in the retrieval

156   algorithm (Chan et al., 2020). Comparisons of TROPOMI $tropNO_2$ column with Pandora ground

157   station retrievals of tropospheric NO_2 in Helsinki showed that mean relative difference is −28.2%

158   ± 4.8% (Ialongo et al., 2019). Similar comparisons between Pandora ground station retrievals

159   and $tropNO_2$ in Canada for urban (Toronto) and rural (Egbert) stations show that $tropNO_2$ has a -

160   23% to -25% bias for polluted regions and a 7% to 11% high bias in rural region. Sources of

161   error in $tropNO_2$ include altitude dependent air mass factors, stratosphere-troposphere separation

162   of NO_2, a priori NO_2 profile and shape, surface albedo climatology, and calibration errors as a

163   function of view angle (van Geffen et al., 2019; Judd et al., 2020; Ialongo et al., 2019; Zhao et

164   al., 2020; Chan et al., 2020). Judd et al. (2020) showed that the TROPOMI NO_2 validation

165   carried out during the Long Island Sound Tropospheric Ozone Study (LISTOS) experiment

166   showed that the TROPOMI $tropNO_2$ column retrievals have a bias of -33% and -19% versus

167   Pandora and airborne spectrometer retrievals respectively. The biases improve to -19% and -7%

168   when TROPOMI NO_2 algorithm is run with a priori profiles from a regional air quality model

169 indicating that retrievals are very sensitive to a priori profile. One aspect that is not fully

170 explored by Judd et al. (2020) is the influence of aerosols on air mass factor calculations.

171 Research on aerosol impact on air mass factors indicates that the impact of aerosols on NO_2

172 retrieval can vary depending on aerosol type (absorbing or scattering), amount, and vertical

173 location (aerosol mixed in with NO_2 in the boundary layer or is the layer detached from NO_2

174 layer) in the atmospheric column (Tack et al., 2019; Judd et al., 2019; Liu et al., 2020; Lin et al.,

175 2014).

176   For this analysis, the pixel level NO_2 data were rotated to orient the pixels in the

177 downwind direction and remapped to 5 km x 5 km fixed grids prior to computing mean values

178 around major cities for which on-road emissions data are available. Average NO_2 was computed

179 within 100 km in the downwind direction from the city center, 50 km upwind direction, and $\pm$ 50

180 km in the cross-wind direction. In computing daily mean values for a location of interest, we

181 used a criteria of having a minimum 25% of the pixels with high quality NO_2 retrieval in each

182 grid. The data for January to February 2020 is considered BAU), the data for 15 March to 30

183 April 2020 is considered the lockdown period, and the data for 1 May to November 2020 is

184 considered as representing the post lockdown time period. The Level 2 TROPOMI NO_2 data

185 were downloaded from the European Space Agency datahub

186 (https://s5phub.copernicus.eu/dhus/#/home).

187   The TROPOMI data is available only from mid-2018 to present. We removed the

188 seasonality in tropNO_2 data in two simple ways: by simply taking the difference between 2019

189 and 2020 for the same month so the sun-satellite geometries and weather conditions are similar

190 barring any unusual inter-annual variabilities, and by doing double differencing when changes

191   from one month to the other month needed to be analyzed. The double differencing method is

192   described in section 3.1.

193   ## 2.2.   On-road NOx Emissions
194

195   The on-road emissions are obtained using the Fuel-based Inventory of Vehicle Emissions

196   (FIVE) where vehicular activity is estimated using taxable fuel sales for gasoline and diesel fuel

197   reported at a state-level and downscaled to the urban scale using light- and heavy-duty vehicle

198   traffic count data (McDonald et al., 2014). Once the fuel use is mapped, NO_x emissions are

199   estimated using fuel-based emission factors (in g/kg fuel) based on roadside measurements or

200   tunnel studies (Hassler et al., 2016; McDonald et al., 2012; McDonald et al., 2018). The emission

201   factors are calculated separately for light-duty gasoline vehicles and heavy-duty diesel trucks.

202   The FIVE methodology was developed to derive traffic emissions to study their impact on air

203   quality (Kim et al., 2016; McDonald et al., 2018), but in the case of 2020, the fuel-based

204   methods provide evidence for quantifying the impact of reduced human activity during the

205   lockdown period on air pollutant emissions (e.g., NO_x).

206   Here, we downscale on-road gasoline and diesel fuel sales following McDonald et al. (2014)

207   for our 2019 base year, which is treated as the BAU case. We have chosen to focus on four US

208   urban areas where real-time traffic counting data are publicly available, including the South

209   Coast air basin (Los Angeles county, Orange counties, and portions of Riverside and San

210   Bernardino counties), San Francisco Bay Area (Marin, Sonoma, Napa, Solano, Contra Costa,

211   Alameda, Santa Clara, San Mateo, and San Francisco counties), New York City (Richmond,

212   New York, Kings, Queens, and Bronx counties), and Atlanta metropolitan region (Cherokee,

213   Clayton, Cobb, Coweta, Dekalb, Douglas, Forsyth, Fulton, Gwinnett, Henry, Rockdale, and

214   Spalding counties). We also include one rural region for contrast, the San Joaquin Valley in

215   California (Fresno, Kern, Kings, Madera, Merced, San Joaquin, Stanislaus, Tulare counties). For

216   the BAU case, we account for typical seasonal and day-of-week activity patterns of light- and

217   heavy-duty vehicles separately). For the COVID-19 case, we scale the January BAU emissions

218   case with real-time light- and heavy-duty vehicle traffic counting data for the year 2020, which

219   are described in Harkins et al. (2020, to be submitted). Light-duty vehicle counts are used to

220   project on-road gasoline emissions and heavy-duty truck counts for on-road diesel emissions

221   during the pandemic.

222   To estimate NO_x emissions, the FIVE NO_x emission factors have been updated to 2019 based

223   on the regression analyses of roadway studies (Hassler et al., 2016; McDonald et al., 2012;

224   McDonald et al., 2018), and we use a value of running exhaust emission factors of 1.7 ± 2 g

225   NO_x/kg fuel and 12.4 ± 1.9 g NO_x/kg fuel for on-road gasoline and diesel engines, respectively.

226   Cold-start emissions are scaled relative to the running exhaust emissions based on the EPA

227   MOVES2014 model (EPA, 2015). We use the 2019 NO_x emission factor for both the BAU and

228   COVID-19 adjusted cases. Thus, the differences in the BAU and COVID-19 cases in are only

229   due to changes in traffic activity. We use the same emission factor for 2019 and 2020 because

230   past studies have shown during the 2008 Great Recession the turnover of the vehicle fleet and

231   corresponding reductions in emission factors are slower). Total on-road NO_x emissions are the

232   sum of emission estimates for light-duty vehicles with heavy-duty trucks. The off-road mobile

233   source emissions are not included in the dataset. In cities, on-road transportation accounts for as

234   much as 75% of the NO_x emissions (Kim et al., 2016), and is a critical emissions sector to

235   quantify.

236   Uncertainties in FIVE on-road emission estimates arise from non-taxable fuel sales

237   associated with off-road machinery, and mismatches in where fuel is sold and where driving

238   occurs, though diesel fuel sales reports are adjusted based on where long-haul trucking occurs

239   (McDonald et al., 2014). However, the main source of uncertainty is the accuracy of fuel-based

240   emissions factors used to calculate co-emitted air pollutant species (McDonald et al., 2018). In

241   general, there has been a downward trend in on-road NO_x emissions over multiple decades

242   (Hassler et al., 2016; McDonald et al., 2012), although there are questions about the rate of

243   decrease in more recent years (Bishop and Haugen, 2018; Jiang et al., 2018).

244   ### 2.3.   Power Plant NO_x Emissions

245   The daily power plant NO_x emissions were obtained from the US Environmental Protection

246   Agency (EPA) Continuous Emissions Monitoring System (https://www.epa.gov/airmarkets) and

247   the energy generation/consumption statistics were obtained from the Energy Information

248   Administration (eia.gov). Unlike the traffic emissions, power plant emissions did not change

249   much during the lockdown. Power generation from fossil fuels dropped from 38,332 Gwh in

250   March to 29,872 Gwh in April and rebounded to pre-pandemic levels by June. The total NO_x

251   emissions in the US from power plants dropped from 54,531 tons in March to 44,016 tons in

252   April, a 19% decrease. This may seem like a big drop in production but the absolute values are

253   quite small. For example, NO_x emissions from power plants within the 75 km of Los Angeles

254   emitted only 20 tons in March 2020. In contrast, on-road emissions from vehicles in the Los

255   Angeles area alone emitted nearly 5,367 tons of NO_x. The power plant NO_x emissions in the US

256   have decreased substantially over the last two decades; they dropped from 6.4 to 0.88 million

257   short tons annually from 1990 to 2019. This is due to the shift in relying on fossil fuels to other

258   alternate energy sources for power generation. For example, the use of coal as a source of

259   electricity generation went down from 51% in 2001 to 23% in 2019 while the natural gas as a

260   source increased from 17% in 2001 to 38% in 2019. In our analysis, comparing and contrasting

261   NO_x emissions from on-road traffic and power plants for the six locations of interest, we

262   considered only the power plants still operating using coal as a source and are within 75 km

263   radius of the center of the city location being analyzed.

264   **2.4.   Suomi National Polar-orbiting Partnership Visible Infrared Imaging Radiometer**
265   **Suite (SNPP VIIRS)**
266

267   NOAA currently has two VIIRS instruments in orbit - one on SNPP launched on 28

268   October, 2011 and one on NOAA-20 launched on 18 November, 2017. The two VIIRS

269   instruments continuously observe the Earth with a 50-minute time difference and provide aerosol

270   optical depth (AOD) retrievals for cloud/snow-free scenes during the sunlit portion of the

271   day. The VIIRS instruments have 22 bands with 16 of the bands in the visible to long-wave

272   infrared at moderate resolution (750m), five bands at imager resolution (375m) covering 0.64μm,

273   0.865μm, 1.6μm. 3.74μm, and 11.45μm, and one broad Day-Night-Band (DNB) band centered at

274   0.7μm. The NOAA AOD algorithm over ocean is based on Moderate Imaging

275   Spectroradiometer (MODIS) heritage and over land, the algorithm derives AOD for both dark

276   targets as well as bright surfaces (Levy et al., 2007; Laszlo and Liu, 2016; Zhang et al., 2016;

277   Huang et al., 2017). For this study, we used SNPP VIIRS AOD because SNPP flies in formation

278   with S5P TROPOMI with less than three minute difference in overpass time with a local equator

279   crossing time of 1:30 PM. The SNPP VIIRS AOD product has been extensively validated by

280   comparing it to Aerosol Robotic Network (AERONET) AODs and the VIIRS 550nm AOD is

281   shown to have a global bias of -0.046±0.097 for AODs over land less than 0.1 and for AODs

282   between 0.1 and 0.8, the bias is -0.194±0.322. In the U.S., for VIIRS AODs ranging between 0.1

283   and 0.8, the bias is -0.008±0.089 and for AODs greater than 0.8, the bias is about 0.068±0.552

284   (Zhang and Kondragunta, 2021). For the analysis of AOD data in this study, we remapped the

285   high quality (Quality Flag equals 0) 750m resolution retrievals to 0.05^{o} x 0.05^{o} resolution with a

286   criteria that for a grid to have a mean AOD value, there should be a minimum of 20% 750m

287   pixels with high quality AODs.

288   ## 2.5.   Unemployment Rate
289

290   The civilian labor force and unemployment estimates for metropolitan areas were obtained

291   through the Local Area Unemployment Statistics (LAUS) provided by the Bureau of Labor

292   Statistics (bls.gov). The LAUS program is a federal-state cooperative effort in which monthly

293   estimates of total employment and unemployment are prepared for over 7,500 areas including

294   metropolitan areas. The seasonal adjustments are carried out by the Current Employment

295   Statistics State and Area program (CES) with statistical technique SEATS, or Signal Extraction

296   in ARIMA (Auto Regressive Integrated Moving Average) Time Series. These datasets are

297   smoothed using a Reproducing Kernel Hilbert Space (RKHS) filter after seasonal adjustment.

298   The details of the data collection, processing and release can be found at

299   https://www.bls.gov/lau/laumthd.htm. The data for January to November 2020 are used in this

300   study. To compare the NO_2 variation in the metropolitan areas, the TROPOMI $tropNO_2$

301   column amounts were averaged inside each metropolitan area. The 1:50,000 polygon shape files

302   were used to test if a TROPOMI pixel is inside or outside a metropolitan area. The shape files

303   are from United States Census Bureau (https://www.census.gov/geographies/mapping-files/time-

304   series/geo/cartographic-boundary.html).

305   ## 2.6.   Matchup Criteria
306

307   The NO$_2$ data were matched to the on-road mobile emissions data for statistical and trend

308   analysis with certain criteria. Prior to generating the matchups, rotated wind analysis was carried

309   out on the original pixel level data. It is important to do this when sampling the satellite data

310   because the NO$_2$ concentrations accumulate in the cities when wind speed is low and disperse

311   away from the city when wind speed is high. The satellite data are observed once a day in the

312   mid-afternoon whereas on-road mobile emissions represent daily values. To minimize sampling

313   differences, it is common to rotate the satellite pixel-level data in the direction of the wind

314   (Fioletov et al., 2015; Lorente et al., 2019; Goldberg et al., 2019; Zhao et al., 2020). We used the

315   European Center for Medium range Weather Forecast (ECMWF) Re-Analysis (ERA5) 30-km

316   resolution global wind fields (Hersbach et al., 2020). To do the wind rotation, each TROPOMI

317   pixel was collocated to ERA5 with tri-linear interpolation method in both temporal and

318   horizontal directions. The wind profiles were merged to the location of the TROPOMI pixel

319   center. The east-west (U) and north-south (V) wind speed components were averaged through

320   the vertical distribution within the bottom 100 hPa, approximated to be within the boundary

321   layer. Then, each TROPOMI pixel was rotated and aligned with the average wind direction from

322   the city center. The rotated pixels are gridded with 5 km x 5 km resolution to generate monthly

323   mean values for correlation analysis with on-road NOx emissions.

324   Once the pixels are rotated, they are sampled for 100 km in the downwind direction, 50 km

325   in the upwind direction, and cross-wind direction. This way, the elevated concentrations of NO$_2$

326   moving away from the city in the downwind direction are captured. Figure 1a shows an example

327   of the TROPOMI NO$_2$ tropospheric column amount for California with Los Angeles as the

328   focus. The NO$_2$ data shown are monthly mean values for January 2020 remapped to a fixed grid.

329   The black rectangle shows the area of interest over Los Angeles that we want to compare with

330   on-road emissions. The ERA5 wind vectors are plotted on the NO_2 map to show wind direction.

331   To do the wind rotation, daily NO_2 pixel level data are first remapped to a 5 km x 5 km fixed

332   grid resolution. The grids are then rotated to align with the wind direction with downwind

333   direction pointing North (Figure 1b). The daily rotated grid values of NO_2 in 5 km x 5 km are

334   averaged over a month to generate a monthly mean. The monthly mean values can vary quite a

335   bit depending on missing data due to screening for high quality data as well as cloud cover. In a

336   given month, the number of pixels with valid retrievals for a particular city can vary from 2% to

337   100% depending on cloud and snow cover, and the mean value varies depending on the location

338   of the missing values, if they are in the center of the city where NO_2 is usually high or on the

339   edges of the city where NO_2 values can be low depending on wind speed and direction. In our

340   analysis for this study, prior to computing monthly mean, the criteria we employed is that on a

341   given day, there should be a minimum of 25% of the pixels in a region selected for matchups of

342   satellite data should have valid retrievals. The 25% threshold is a reasonable compromise

343   because any value higher than that will reduce the sample size (number of days included in the

344   monthly mean).

3. Results

3.1. Deseasonalizing tropNO$_2$ data

348   As already shown by many research studies, the global tropNO$_2$ column amounts dropped in

349   coincidence with partial or complete lockdowns during the height of the COVID-19 pandemic in

350   different parts of the world and in the US. In order to remove the seasonality from the signal,

351   researchers have adopted different approaches including the use of numerical models to simulate

352   the seasonality (e.g., Goldberg et al., 2020; Silver et al., 2020; Liu et al., 2020). Seasonality has

353   to be accounted for because in the northern hemisphere winter months, NO_2 amounts are higher

354   than in summer months due to which during the transition from winter to summer, NO_2 amounts

355   are higher in February than in March. In our study, we used a double differencing technique to

356   account for seasonality. Consistent with Goldberg et al. (2020), we used 1 January to 29

357   February 2020 as pre-lockdown time period and 15 March to 30 April as lockdown time period.

358   The difference in mean $tropNO_2$ between lockdown and pre-lockdown is referred to as

359     $2020\Delta NO_2$. For the same two corresponding time periods in 2019, the difference in mean

360     $tropNO2$ is $2019\Delta NO_2$. Then, the difference of $2019\Delta NO_2$ and $2020\Delta NO_2$ was computed to

361   tease out the changes in NO_2 due to reductions in emissions during the lockdown (ΔNO_2). It

362   should be noted though that the double differencing only removes the seasonality and does not

363   fully account for differences in meteorological events such as precipitation or anomalously cold

364   or hot conditions in one year versus the other but on a monthly time scale they are minimized.

365   Figure 2a-b shows $2019\Delta NO_2$ and $2020\Delta NO_2$ which includes changes due to seasonality and

366   any changes to emissions either from natural sources such as fires or anthropogenic

367   urban/industrial sources. Figure 2c shows ΔNO_2 for the CONUS due to just changes in

368   emissions between the pre-lockdown and lockdown time periods in 2020 with the seasonality

369   removed.   Comparing Figure 2a and 2b, one can deduce that reductions in $tropNO_2$ between pre-

370   lockdown and lockdown is much stronger in 2020 compared to 2019. However, the double

371   difference plot in Figure 2c shows how much of that reduction seen in $2020\Delta NO_2$ (Figure 2b) is

372   due to changes in traffic emissions. The NO_2 changes are smaller in Figure 2c than in Figure 2b,

373   both in magnitude as well as spatial extent of the reductions.

374   The lockdown measures in most states in the US began in the middle of March 2020. The

375   first state to institute stay at home measures was California on 19 March and the last state to

376   enforce was Missouri on 6 April. The cities/regions with worse traffic related ozone pollution

377   levels based on the monitoring data from 2016-2018 compiled by the American Lung

378   Association and the duration for which they were in a lockdown is shown in Table 1. For

379   regions that fall into different states (e.g., Washington-Baltimore-Arlington), the dates for the

380   state that had the longest duration of lockdown are listed in the table. Most states were in a

381   lockdown mode only for one to two months and given the varying nature of the lockdown in

382   different parts of the country, we treated 15 March and 30 April as lockdown months.   As shown

383   in Figure 2a, 2019ΔNO_2 is positive in some areas and negative in some areas whereas in 2020

384   (Figure 2b), large negative values (reductions) are observed in most of the CONUS except in the

385   Great Plains region and the Pacific North West. These reduced $tropNO_2$ amounts are attributed to

386   reduced emissions due to lockdowns. Changes in the rural areas (either positive or negative) of

387   the US could be due to changes to natural sources such as soil and lightning NO_x emissions.

388   ### 3.2.   On-road NO_x emissions and $tropNO_2$
389

390   Focusing on the regions of interest with on-road NOx emissions available for this study, we

391   calculated reductions in $tropNO_2$ for Los Angeles, Atlanta, San Francisco, San Joaquin Valley,

392   and New York City. The largest reductions in $tropNO_2$ were observed for New York City (-28%)

393   and the lowest were observed for San Francisco (-21%). For Los Angeles, the straight difference

394   between pre-lockdown and lockdown in 2020 shows reductions of ~81 $\mu moles/m^2$ when in fact

395   NOx emissions reductions from traffic only likely reduced $tropNO_2$ by 32 $\mu moles/m^2$ which is

396   about 21% as estimated by the double differencing technique (Table2).

397   Goldberg et al (2020) reported $tropNO_2$ reductions of 20.2%, 18%, and 39% for Atlanta,

398   New York, and Los Angeles respectively and their analysis is also for March 15 to April 30,

399   2020 time period. Our analysis shows that $tropNO_2$ reductions for these three cities are 21%,

400   17%, and 22%. Though the methodology used to remove the seasonality is different, the

401   reductions in tropNO$_2$ from our analysis and that of Goldberg et al. (2020) is similar with Los

402   Angeles showing the biggest drop in tropNO$_2$ due to lockdown measures.

403   The goal of this study is, however, not to repeat what other researchers have already

404   reported for the COVID-19 lockdown impacts on tropNO$_2$ using TROPOMI data. What we

405   examined in this study is the trends in on-road and power plant emissions for five different

406   locations (four urban areas and one rural area) to answer the questions: (1) are changes in NOx

407   emissions during the lockdown detectable in TROPOMI tropNO$_2$ data, (2) are the economic

408   indicators consistent with emissions changes, and (3) are the trends reversing with the removal of

409   lockdown measures.

410   Figure 3 shows the time series of on-road mobile (cars and trucks combined) and power plant

411   NO$_x$ emissions for five different cities/regions in the US (Los Angeles, Atlanta, New York, San

412   Joaquin Valley, and San Francisco) from January to November 2020 except for New York City

413   for which the time series ends on 31 August due to the non-availability of traffic data. For Los

414   Angeles, the daily NO$_x$ emissions are near 200 tons/day prior to lockdown with values slightly

415   lower on weekends (~150 tons/day). The Los Angeles basin is home to 17 million people with

416   11.3 million cars; cars, trucks, and other off-road machinery contributing to 80% of the observed

417   NO$_x$ in a typical year according to the 2019 emissions report by South Coast Air Quality

418   Monitoring Division (http://www.aqmd.gov/docs/default-source/annual-reports/2019-annual-

419   report.pdf?sfvrsn=9). Due to the lockdown and stay at home orders, people stopped driving and

420   the NO$_x$ emissions quickly began dropping on 19 March 2020; the NOx emissions begin to

421   increase on 16 April 2020, even before the lockdown was lifted on 4 May. The lowest weekday

422   NO$_x$ emissions, 141.3 tons/day, occurred on 6 April. Even though the NOx emissions begin to

423 recover in the post lockdown time period, they are still lower than the pre-lockdown values.

424 Compared to on-road emissions, power plant emissions are negligible for the Los Angeles area.

425 Power plants in the vicinity of Los Angeles (~75 km radius) emit only ~0.8 tons per day on

426 average compared to 200 tons per day emitted by on-road vehicles during the pre-lockdown on

427 weekdays. On weekends, on-road emissions are lower (~150 to 175 tons/per day depending on

428 whether it is a Saturday or Sunday) due to lower truck traffic (Marr and Harley, 2002), whereas

429 power plant emissions do not have any weekday/weekend differences.

430   The NO_x emissions for the New York area encompass an area covering about 1,213 square

431 kilometers. The city is home to 8.34 million people but there are only 1.9 million vehicles (230

432 cars per 1000 people) because of the reliance on public transportation, a factor of 3 lower than

433 for Los Angeles basin which has 660 cars per 1000 people. Similar to Los Angeles, the NO_x

434 emissions dropped in New York on 21 March when the lockdown measures began. The pre-

435 lockdown levels of NOx emissions are on average ~125 tons/day. It should be noted that New

436 York City is in the downwind region of NOx emissions from New Jersey and Pennsylvania and

437 the recipient of regionally transported pollution (Tong et al., 2008). Unlike the Los Angeles

438 area, the power plant emissions are higher but showed no trend similar to on-road emissions. It

439 is noteworthy that there is a jump in power plant emissions towards the end of June which

440 coincides with the opening of retails on 22 June in New York; the power plant emissions in the

441 New York City are higher in the summer than in winter, associated with increased demand for

442 air conditioning.

443   The NO_x emissions for the metro Atlanta area are similar to New York City but with a weak

444 weekday/weekend cycle. The region encompassing Cherokee, Clayton, Cobb, Coweta, Dekalb,

445 Douglas, Forsyth, Fulton, Gwinett, Henry, Rockdale, and Spalding counties is about 3,695

446   square kilometers and is home to nearly five million people. The pre-lockdown levels of NOx

447   emissions are on average ~125 tons/day. The metro Atlanta region is three times larger than the

448   area covered for the New York City region but the NOx emissions are similar in magnitude. The

449   state of Georgia where Atlanta is located never went into any prolonged lockdown. Though the

450   mayor of Atlanta ordered people not to gather in large groups beginning 15 March and the

451   Governor of Georgia ordered bars and clubs to close on 24 March, schools were not closed until

452   1 April; shelter in place was implemented on 8 April but was lifted immediately with no real

453   lockdown until 1 May through 23 May. Consistent with these policies, the on-road NO_x

454   emissions were lowest on 23 March (88.5 tons/day) and 26 May (74.5 tons/day) and returned to

455   pre-lockdown levels at the start of 1 June. The lowest on-road NOx emission value, 74.5 tons,

456   was observed on 26 May, towards the end of the shelter in place orders. By 1 June, NO_x

457   emissions values returned to normal, pre-lockdown levels in Atlanta.

458   For the pre-lockdown time period, the weekday/weekend difference in NO_x emissions is

459   stronger in New York City than Los Angles and Atlanta areas, due to commuter travel. Mean

460   difference in NO_x emissions between weekdays and Sundays (emissions are the lowest on

461   Sundays of each week) prior to the pandemic related lockdown in the Los Angeles, New York,

462   and Atlanta are 54.4 tons/day (26%), 65.4 tons/day (51%), and 41.1 tons/day (33%) respectively.

463   The San Joaquin valley is a rural area with low on-road and power plant emissions and the

464   data are expected to have a contrast to the urban/industrial locations such as Los Angeles and

465   New York City. The San Joaquin Valley NO_x emissions remained consistent at ~55 tons/day

466   throughout the year with a very weak weekday/weekend cycle. Similar to Los Angeles area, the

467   power plant emissions are insignificant. For the San Francisco Bay area, the on-road NO_x

468   emissions are higher than the San Joaquin Valley region but lower than the Los Angeles area.

469   The daily average NO_x emissions prior to the lockdown were ~90 tons/day and there was a small

470   drop in emissions (-33.2 tons/day) on 6 April with a trend to return to normal by mid-April. The

471   post lockdown NOx emissions are lower than pre lockdown values for San Francisco as well.

472   3.3.   Correlation between on-road NO_x emissions and tropNO$_2$

473

474   Given the knowledge of changes in on-road emissions in five locations due to lockdown, we

475   wanted to examine if tropNO$_2$ shows similar behavior by exhibiting a linear relationship and

476   demonstrate that the time period for which lowest NO_x emissions were observed in traffic data

477   also corresponds to the lowest observed tropNO$_2$ data. Additionally, we wanted to check if the

478   post lockdown recovery in traffic emissions is reflected in tropNO$_2$ data. We first examined the

479   direct relationship between daily tropNO$_2$ and daily on-road NO_x emissions for the five locations

480   but only the analysis for Los Angeles is shown in Figure 4. The tropNO$_2$ and NO_x emissions for

481   January and February 2020, representing the pre-lockdown phase, and for March through

482   November 2020 are shown in Figure 4a and Figure 4b respectively. Again, the daily NO_x

483   emissions data are for the Los Angeles basin. The coincident observations of tropNO$_2$ amount

484   sampled in the predominant direction of wind are linearly correlated with on-road emissions but

485   the correlation is weak (r=0.39). The traffic emissions fall into three clusters corresponding to

486   emissions on Sundays (~150 tons/day), Saturdays (~180 tons/day), and weekdays (~199

487   tons/day) with minimal variability in each cluster whereas tropNO$_2$ amount varied between 50

488   and 225 μmoles/m^2.

489   The variability in tropNO$_2$ can be present due to different reasons. First, the day to day

490   variability in cloud cover can lead to gaps in data. We used the recommended quality flag

491   threshold of 0.75 to screen out the data that has potential contamination from clouds but this

492   strict screening reduces the number of retrievals for a given location. Second, there is also

493   variability in the background NO_2 contribution to the tropospheric NO_2 column due to which

494   column NO_2 does not correlate well with NO_x emissions from sources on the ground. We

495   analyzed the background NO_2 signal in the tropospheric column amount for TROPOMI for 2019

496   and 2020 using Silvern et al. (2019) method and found it to be higher in the winter due to longer

497   lifetime (lower temperature, weak photolysis, stronger wind dispersion, and less wet scavenging)

498   and lower in the summer with monthly mean values ranging between 15 and 20 $\mu moles/m^2$.

499   Sources of background NO_2 are soil emissions of NO_x which are amplified after precipitation

500   events, lightning produced NO_x, and chemical decomposition of peroxyacetyl and alkyl nitrates.

501   When transport of NO_2 from rural areas to urban centers occur, this can enhance the tropNO$_2$

502   values that may not correlate well with NO_x emissions from sources on the ground. Third, wind

503   speed and direction influences the mean tropospheric NO_2 computed for the Los Angeles basin

504   because if the wind speed is high, NO_2 is dispersed and transported away from the city and when

505   the wind speed is low, NO_2 is accumulated over the city. Any variability associated with

506   background NO_2 is detected by TROPOMI and accounted for in the column NO_2 amount that

507   has no relation to the NO_x emissions from the on-road sources on the ground. We did account

508   for the effects of wind in our matchups by sampling the data in the downwind direction but

509   higher wind speeds dilute the NO_2 concentrations observed by TROPOMI. The outliers that

510   indicate tropNO$_2$ values are between 20 and 30 $\mu moles/m^2$ even when on-road emissions are

511   high indicate TROPOMI retrievals that are either sampled after pollutants are washed out of the

512   atmosphere due to rain or on days when wind speeds are unusually high or are noisy and have

513   errors associated with air mass factors and a priori profile. Parker et al. (2020) report that the

514   Los Angeles basin was unusually wet in 2020, especially during the late March and early April

515   2020. Other researchers who correlated daily surface observations of NO_2 and TROPOMI

516   tropNO$_2$ for 35 different stations in Europe reported similar findings and they found that

517   correlation improved after averaging the data to monthly time scales (Ialongo et al., 2020;

518   Cersosimo et al., 2020).

519   The comparison for the lockdown and post lockdown time period of March through

520   November is shown in Figure 4b; the correlation remains the same (r = 0.39) but the one

521   interesting feature is that the tropNO$_2$ and on-road emissions are very small compared to the pre-

522   lockdown scenario. Daily NOx emissions on many days are between 100 and 150 tons after 14

523   March; prior to that in the first 15 days of March, the region was not under stay at home orders.

524   The tropNO$_2$ never goes above 200 μmoles/m^2 for this time period. Compared to pre-lockdown

525   period, the on-road NO_x emissions and tropNO$_2$ values shifted to lower values within each

526   cluster (shown in blue for weekdays, green for Saturdays, and red for Sundays). During the

527   lockdown phase, one would anticipate that there would not be any difference between weekday

528   and weekend emissions but the difference is stark and is reflected in tropNO$_2$ data as well.

529   In order to correlate the changes in on-road NOx emissions to changes in tropNO$_2$ between

530   2019 and 2020 for each of the five regions in this study, we averaged daily NOx emissions

531   values and tropNO$_2$ values for each month (January to November) and created an average value

532   of all the five regions combined for each month. Figure 5a shows the monthly mean trend plot

533   ΔNO_x and ΔtropNO$_2$ for January to November where we see on-road emissions and tropNO2

534   drop steadily and hit the lowest values in March and April, consistent with lockdown measures.

535   The recovery begins in May and continues to November for on-road emissions but not

536   completely to the pre-lockdown levels. However, the ΔtropNO$_2$ trend plot shows recovery up to

537   August and then begins to show a decline from September to November. This decline in

538   tropNO$_2$ is coming from Los Angeles and San Francisco. The reason for this drop is currently

539   unclear and warrants further investigation but some initial analysis presented in Section 3.4

540   suggests there was likely an influence of biomass burning emissions on the Los Angeles area in

541   September 2020. Figure 5b shows the correlation of on-road NOx emissions changes (ΔNO_x)

542   between 2020 and 2019 with the difference in tropNO$_2$ amounts between 2020 and 2019

543   (ΔtropNO2). The NO$_x$ emissions were lower in 2020 compared to 2019 for all the months and

544   all the cities. The positive linear correlation (r = 0.68) suggests that tropNO$_2$ observations

545   captured the changes in on-road emissions and can be used to study the changes in NOx

546   emissions due to traffic elsewhere in the US where we do not have observations from the ground.

547   Even though traffic emissions are the dominant source for NOx, there are power plants in the

548   vicinity of the cities emitting NOx on a continuous basis and unlike traffic emissions they do not

549   exhibit a weekday/weekend cycle. Figure 6 shows a map of tropospheric NO$_2$ for Quarter 2

550   2020 (April/May/June) with on-road emissions and power plant emission for each of the five

551   cities as stacks. The locations of power plants in other parts of the country are circled in pink

552   color, indicating that these power plants emit greater than 1500 tons in a given quarter; power

553   plants with lower monthly NOx emissions < 1500 tons are not highlighted on the maps. It is

554   difficult to isolate the NO$_2$ plumes from power plants in urban areas in the TROPOMI NO$_2$ map

555   as the NO$_x$ emitted from the power plants mixes and becomes indistinguishable from on-road

556   emissions. Consistent with this analysis, changes in NO$_x$ emissions between 2020 and 2019 for

557   power plants within 75 km of each of the five cities (New York, Atlanta, San Francisco, Los

558   Angeles, and San Joaquin Valley) correlated weakly with changes in tropNO$_2$ (Pearson

559   correlation coefficient = 0.35); power plant NO$_x$ emissions can explain only 12% of the

560   variability seen in tropNO$_2$ (Figure 7). The changes in power plant emissions were higher in

561   2020 compared to 2019 for some plants and lower for some but mostly varied between ±20

562   tons/day whereas the on-road emissions reduced by about ~80 tons/day.

563   ### 3.4. NO_x photochemistry

564

565   The premise for the impact of NO_x emissions reductions on improved air quality due to

566   reduced human activity during the lockdown period depends on how the photochemical

567   processes changed compared to the BAU scenario. It is known that in the Los Angeles area,

568   reductions of NO_x emissions on the weekend due to reduced traffic compared to weekdays has

569   led to an increase in ozone due to less NO_x available to remove ozone via titration (Baider et al.,

570   2014). Parker et al. (2020) report that during the April to June 2020, when NO_x emissions were

571   reduced substantially due to a 50% drop in traffic, there was a spatial modification of ozone

572   production but not necessarily a drop, suggesting larger and more targeted NO_x reductions are

573   needed in the Los Angeles area in order to consistently reduce ozone. While most of the NOx in

574   the Los Angeles area comes from cars and trucks, only 25% of VOC emissions come from cars

575   and trucks; sources of VOCs are mostly area and biogenic sources (Parker et al., 2020).

576   McDonald et al. (2018) and Qin et al (2021) suggest the importance of volatile chemical

577   products as sources of anthropogenic VOCs in the Los Angeles impacting both ozone and

578   secondary organic aerosol. Most analysis using the satellite data are focusing on TROPOMI

579   NO_2 and attributing the reductions of NO_x emissions to improved air quality; the reductions in

580   VOC emissions are largely unknown, especially of non-vehicular sources. The aerosol

581   formation (nitrate and organic aerosols) is driven by NO_x, VOCs, and ammonia emissions and if

582   the photochemical processes are in NO_x limited or VOC limited regime. One complicated factor

583   for aerosols is the transport of smoke aerosols if fires are burning upwind of the city. We

584   established some baseline photochemical regime by calculating weekly correlation between

585 AOD and NO_2 and obtaining the slope for each week over one year in 2019 to document the

586 changes in slope as a function of time during the year (Figure 8a-c); Figure 8a-b show how

587 slopes are derived using the scatter plot between VIIRS AOD and TROPOMI tropNO2 for one

588 week in September 2019 and in 2020 as an example. For 2019, when the fire season was not a

589 major contributing factor, the slopes are small in the winter months and slowly increase towards

590 the summer. This is consistent with the knowledge that ammonium nitrate formation peaks in

591 the summer due to the availability of ammonia from increased agricultural activity and higher

592 volatility associated with higher temperatures (Schiferl et al., 2014).

593   The black curve in the figure is a polynomial fit to the 2019 AOD-tropNO$_2$ slope data and

594 represents the increase in the rate of nitrate aerosol formation from winter to summer, and

595 decrease from summer to winter. The AOD to tropNO$_2$ slopes for the year 2020 are shown as

596 red dots and any significant sudden increase in the slope is interpreted as the influx of

597 transported aerosol into the domain. The weekly scatter plots of AOD and AOD-tropNO$_2$ for

598 September 2019 and 2020 in Figure 8a-b show that the tropNO$_2$ values in both years ranged

599 between 30 and 120 μmoles/m^2 whereas AOD values in 2020 were much higher (between 0.2

600 and 0.9) compared to values in 2019 that were only between 0.1 and 0.2. The AOD values

601 typically range between 0 and 1, with higher AODs typically observed in the presence of

602 biomass burning smoke or dust storms. The values in 2019 are akin to photochemically

603 produced aerosols whereas the high values in 2020 indicate aerosols due to photochemically

604 produced aerosols plus any transported aerosol from locations upwind of Los Angeles.

605   3.5.   Economic activity indicators and tropNO$_2$

606

607   Because of the lockdown measures and work from home policies for majority of the

608   workplaces in the US, the service industry has taken a hit and the unemployment rate has risen.

609   The US unemployment rate increased from about 4.4% in March to 14.7% in April during the

610   first phase of lockdown. The unemployment rate nationwide improved as the year went by but

611   certain parts of the country continued to be under very high unemployment rate throughout 2020

612   (Figure 9). Amongst the employed, 28% of employees continue to work from home as of

613   November indicating that below normal NO_x emissions data are to be expected. The correlation

614   between unemployment rate and tropNO$_2$ for metropolitan areas with pre-pandemic civilian

615   labor force greater than two million is negative for the second and third quarters (the regression

616   line shown in Figure 9 is for second quarter data). The unemployment rate combined with

617   telework policies have contributed to reduced NO_x emissions and thus the lower tropNO$_2$ values

618   across the US. This is similar to the positive correlation between Gross Domestic Product (GDP)

619   and tropNO$_2$ reported by Keller et al. (2020). Cities such as Phoenix, AZ, Minneapolis, MN,

620   Dallas and Houston, TX, and Chicago, IL show no change or slight increase in tropNO$_2$ in 2020

621   compared to 2019 though unemployment rate in 2020 is much higher compared to 2019.

4. Discussion

623

624   The TROPOMI tropNO$_2$ data captures the day to day variability but due to cloud cover and

625   uncertainties associated with assumptions such as a priori profile and lower sensitivity to near

626   surface NO_2, on certain days the retrievals do not adequately represent the changes in near

627   surface NO_2. Our analysis shows that the data reflect the NO_2 variability very well on monthly

628   scales and even on weekly scales, to the extent that even weekday/weekend cycles are

629   noticeable.   When using the TROPOMI tropNO$_2$ data, we wanted to establish that it not only

630   shows the reductions/drop in tropNO$_2$ due to reductions in on-road emissions but that the trend

631   during post-lockdown recovery can be detected as well. Therefore we examined the trends in

632   on-road and power plant emissions for five different locations (four urban areas and one rural

633   area) to answer the questions: (1) are changes in NOx emissions during the lockdown detectable

634   in TROPOMI tropNO$_2$ data, (2) are the economic indicators consistent with emissions changes,

635   and (3) are the trends reversing with the removal of lockdown measures in the major metro areas.

636   These locations have diversity from a geographical perspective, are driven by different

637   economies, and experience different meteorology and climate. The inventory from ground

638   monitors for locations nationwide and its analysis is the subject of a different publication. The

639   focus in this paper is to corroborate trends seen in satellite data with ground observations.

640   The spatial and temporal analysis, relating indicators of human activity during and prior to

641   COVID-19 lockdown with air quality shows that while power plant emissions changes were not

642   drastic compared to on-road emissions, the on-road emissions in the four urban and one rural

643   location dropped coinciding with lockdown start date and duration. The changes in on-road NOx

644   emissions correlated with tropNO$_2$ changes for these five locations, giving confidence to use

645   tropNO$_2$ data in other parts of the CONUS to draw conclusions about relating changes in

646   tropNO$_2$ to economic activity changes. We found that the weekday-weekend differences were

647   pronounced in on-road emissions and tropNO$_2$ data with the lowest values of on-road NOx were

648   all on weekends even during the pandemic related lockdown periods. The unemployment rate

649   and its increase during the lockdown and post lockdown period appears to also be a good proxy

650   for economic activity and correlated well with decrease in tropNO$_2$ changes. At the height of the

651   pandemic related lockdown in second quarter 2020, the unemployment rate increase was as high

652   as 17% in populated metropolitan areas and even at the end of the third quarter in 2020, the

653   unemployment increase is ~10%. The first quarter unemployment showed no relationship to

654   tropNO$_2$ as expected because it was constant at ~5% and did not vary.

655   The satellite data must be analyzed by considering various quality flags and understanding

656   the limitations of the algorithm. It is likely that by using the quality flag > 0.75, we were

657   conservative in the use of TROPOMI data but the extremely low daily tropNO$_2$ values on certain

658   days even when on-road NO$_x$ emissions were high is indicative that the data are more

659   interpretable when averaged to weekly or monthly time scales. For tropNO$_2$ retrievals that have

660   quality flags between 0.5 and 0.75, suggesting cloud contamination, we can look at coincident

661   high resolution (750m) VIIRS cloud mask product to analyze TROPOMI flags for cloud

662   contamination. This analysis will help us improve our analysis using the daily tropNO$_2$ retrievals

663   by either including more retrievals or removing some retrievals from the matching with on-road

664   emissions data.

665   ## 5. Conclusions
666
667   It has already been established by numerous research studies that reduced traffic (on-

668   road) and industrial emissions led to improved air quality during the lockdown measures

669   implemented by various countries across the globe. However, most studies used mobility data as

670   a proxy for reduced human activity to interpret satellite observations of tropNO$_2$ but did not

671   directly relate the reduced on-road emissions with reduced air quality observations. Here, for

672   the first time we directly correlate on-road NO$_x$ emissions data to TROPOMI tropNO$_2$ in four

673   metropolitan and one rural areas in the US. For this, we used TROPOMI tropNO$_2$, VIIRS AOD,

674   on-road NOx emissions, and unemployment rates to develop a comprehensive analysis for 2019

675   and 2020. Where needed, we conducted rotated wind analyses to correctly sample and match the

676   on-road NOx emissions with tropNO$_2$ data, developed a novel way of deseasonalizing tropNO$_2$

677   data, and used changes in unemployment rate data as an indicator for economic activity.

678   Our analysis of reductions in on-road NO$_x$ emissions from light and heavy duty vehicles

679   derived from fuel sales data showed a reduction from 9% to 19% between February and March at

680   the onset of lockdown in the middle of March in most of the US and between March and April,

681   the on-road NO$_x$ emissions dropped further by 8% to 31% when lockdown measures were the

682   most stringent. These precipitous drops in NO$_x$ emissions correlated well with tropNO$_2$.

683   Further, the changes in tropNO$_2$ across the continental U.S. between 2020 and 2019 correlated

684   well with changes in on-road NO$_x$ emissions (Pearson correlation coefficient of 0.68) but

685   correlated weakly with changes in emissions from the power plants (Pearson correlation

686   coefficient of 0.35). These findings confirm the known knowledge that power plants are no

687   longer a major source of NO$_2$ in urban areas of the United States. As the US entered into a post-

688   pandemic phase between May and November 2020, the increased mobility resulted in increased

689   NO$_x$ emissions nearly to the pre-lockdown phase but not entirely back to 100%. These changes

690   are reflected in the tropNO$_2$ data except that for Los Angeles and San Francisco, the tropNO$_2$

691   diverged from on-road NO$_x$ emissions that needs further inquiry. The negative correlation

692   between changes in tropNO$_2$ in 2020 compared to 2019 and increased unemployment rate

693   indicates that with increased unemployment rate combined with telework policies across the

694   nation for non-essential workers, the NO$_2$ values decreased at the rate of 0.8 μmoles/m^2 decrease

695   per unit percentage increase in unemployment rate.

696   Across the CONUS we found positive spatial correlation between S5P TROPOMI NO$_2$ and

697   SNPP VIIRS AOD measurements in these urban regions indicating common source sectors for

698   NO$_2$ and aerosols/aerosol precursors. Once the data are averaged into weekly means and

699   temporally correlated and weeks when transported smoke mixes in with locally produced

700   emissions are removed, there is a negative correlation between AOD and tropNO$_2$ indicating that

701   photochemical conversion of NO$_2$ to nitrate aerosol is being captured in this analysis. This

702   methodology of screening for fire events influencing aerosol concentrations over urban/industrial

703   regions also helps with analyzing changes in aerosols due to emissions reductions. This is the

704   subject of a different manuscript that is currently in preparation. The COVID-19 pandemic

705   experience has provided the scientific community an opportunity to identify scenarios that can

706   lead to a new normal urban air quality and if the new normal can be sustained with novel policies

707   such as increased telework policies and a shift towards driving electric cars.

708
709

726   **Author Contributions.** SK conceived the scope of the scientific study and formulated the

727   analysis and wrote the manuscript. ZW conducted the scientific analyses including the

728   generation of the figures used in the manuscript. BM processed and provided the on-road NO_x

729   emissions data and wrote Section 2.2. DLG and DT conducted analysis that helped interpret the

730   features observed in TROPOMI tropospheric NO_2 data shown in Figures 4 and 5 and reviewed

731   the manuscript.

732   **Disclaimer.** The scientific results and conclusions, as well as any views or opinions expressed

733   herein, are those of the author(s) and do not necessarily reflect those of NOAA or the

734   Department of Commerce.

735   **Data Statement.** The publicly available SNPP VIIRS AOD data can be obtained from NOAA

736   CLASS (https://www.avl.class.noaa.gov) and the gridded Level 3 AOD data can be obtained

737   from ftp://ftp.star.nesdis.noaa.gov/pub/smcd/VIIRS_Aerosol/npp.viirs.aerosol.data/epsaot550.

738   The Sentinel 5P TROPOMI NO2 data can be obtained from https://scihub.copernicus.eu/. The

739   on-road NOx emissions data are currently not publicly available as the team is still conducting

740   the analysis for publication purpose.

741

742

743

744

745

746

747
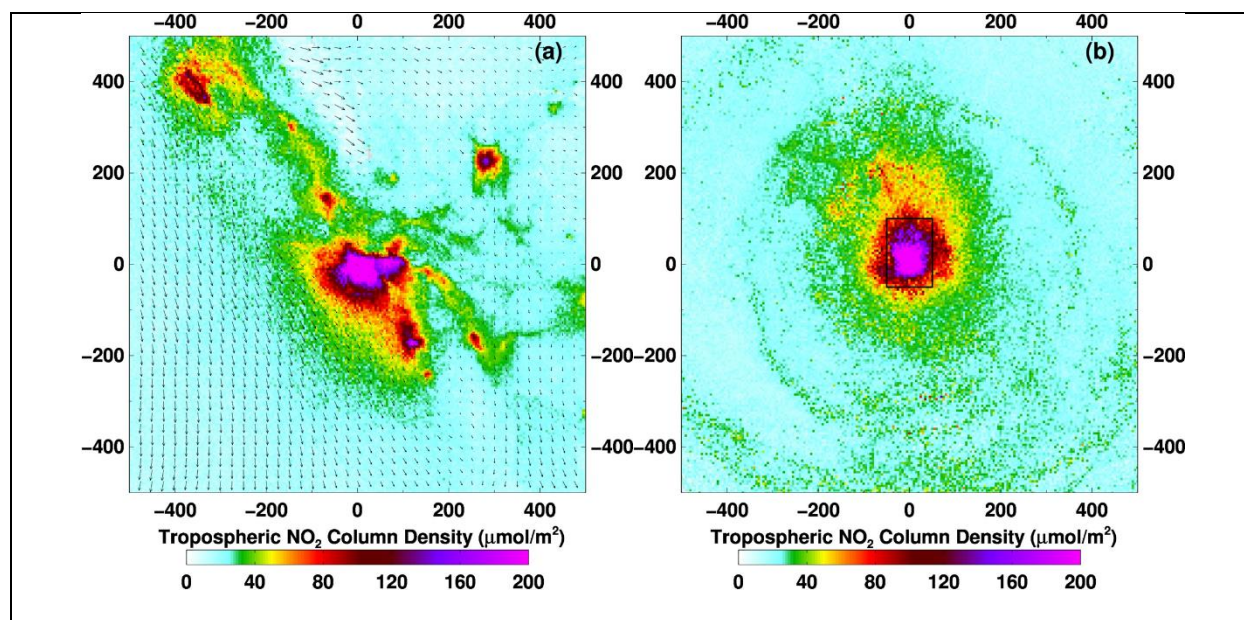
748

749

750

751

752

Figure 1: Sentinel 5P TROPOMI monthly mean NO_2 for January 2020 for California. (a) Original pixel level data remapped to 5 km x 5 km resolution and averaged for the month. The monthly mean ERA5 wind vectors are overlaid on the NO_2 map to indicate the wind direction. (b) Original pixel level NO_2 data remapped to 5 km x 5 km grids and the grids rotated in the direction of the wind using ERA5 wind fields. The downwind direction is shown pointing North. For the monthly mean to be computed, we used a criteria that at least 25% of the days in a month should have retrievals.

753
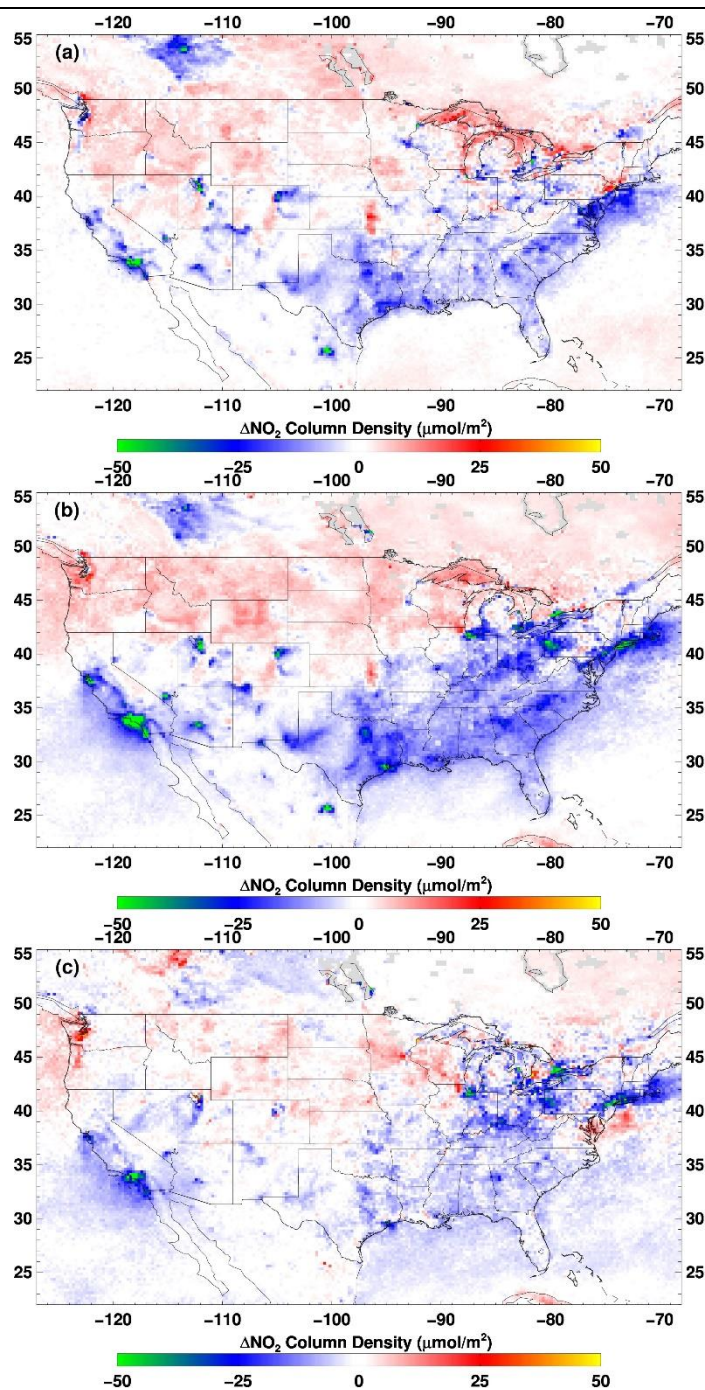
Figure 2: Tropospheric NO_2 changes between pre-lockdown time period (January to February) and lockdown period (15 March to 30 April) for (a) $2019\Delta NO_2$, (b) $2020\Delta NO_2$, and (c) the difference between $2020\Delta NO_2$ and $2019\Delta NO_2$. The double differencing is expected to remove the seasonal differences and provide a realistic estimate of change in $tropNO_2$ due to emissions changes.

Figure 3: Time series of on-road and power plant NOx emissions for different cities from January to November 2020. Note that the time series ends on 31 August for New York City because the traffic count data are not available for September to November.
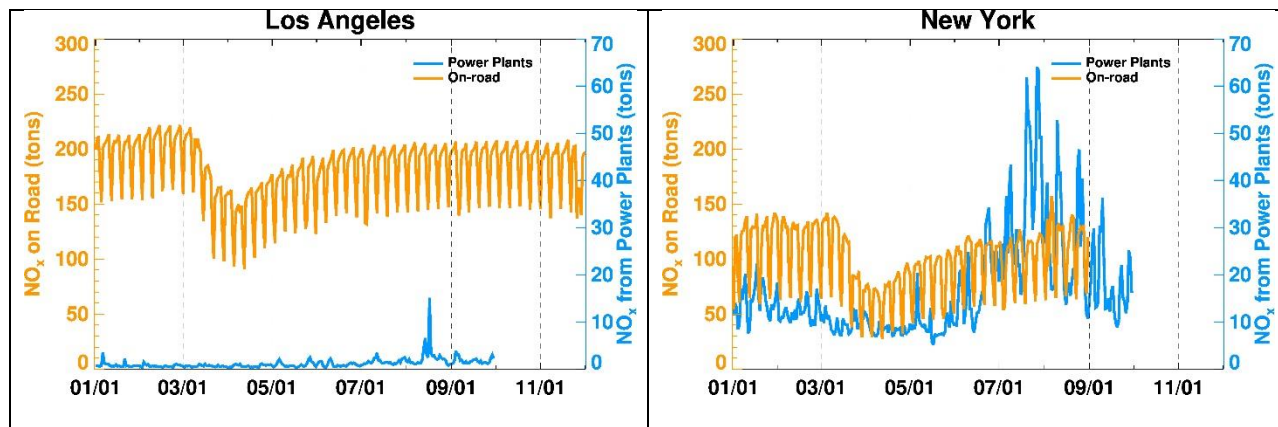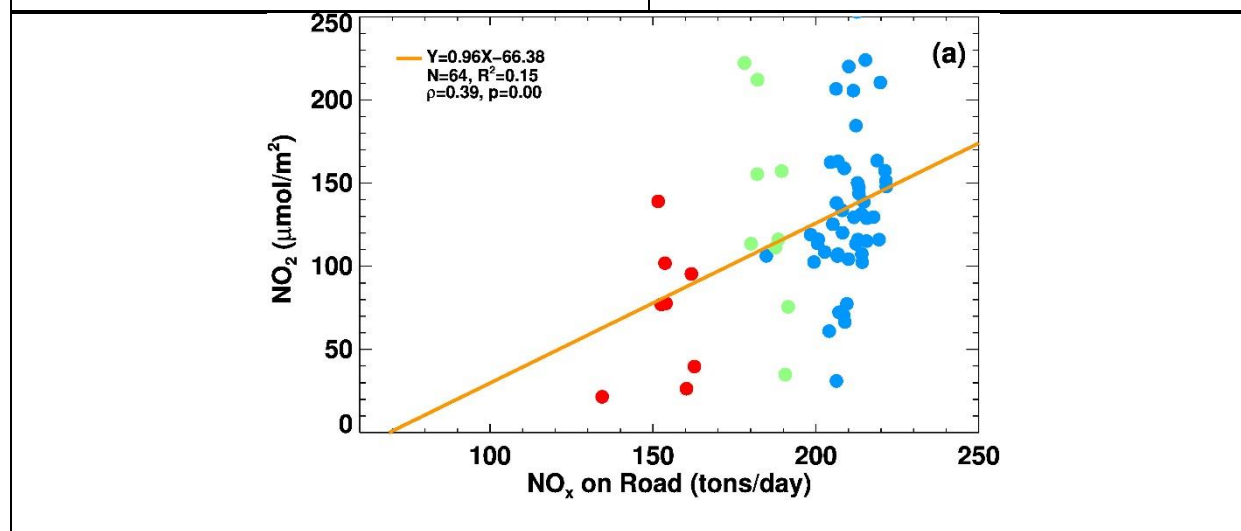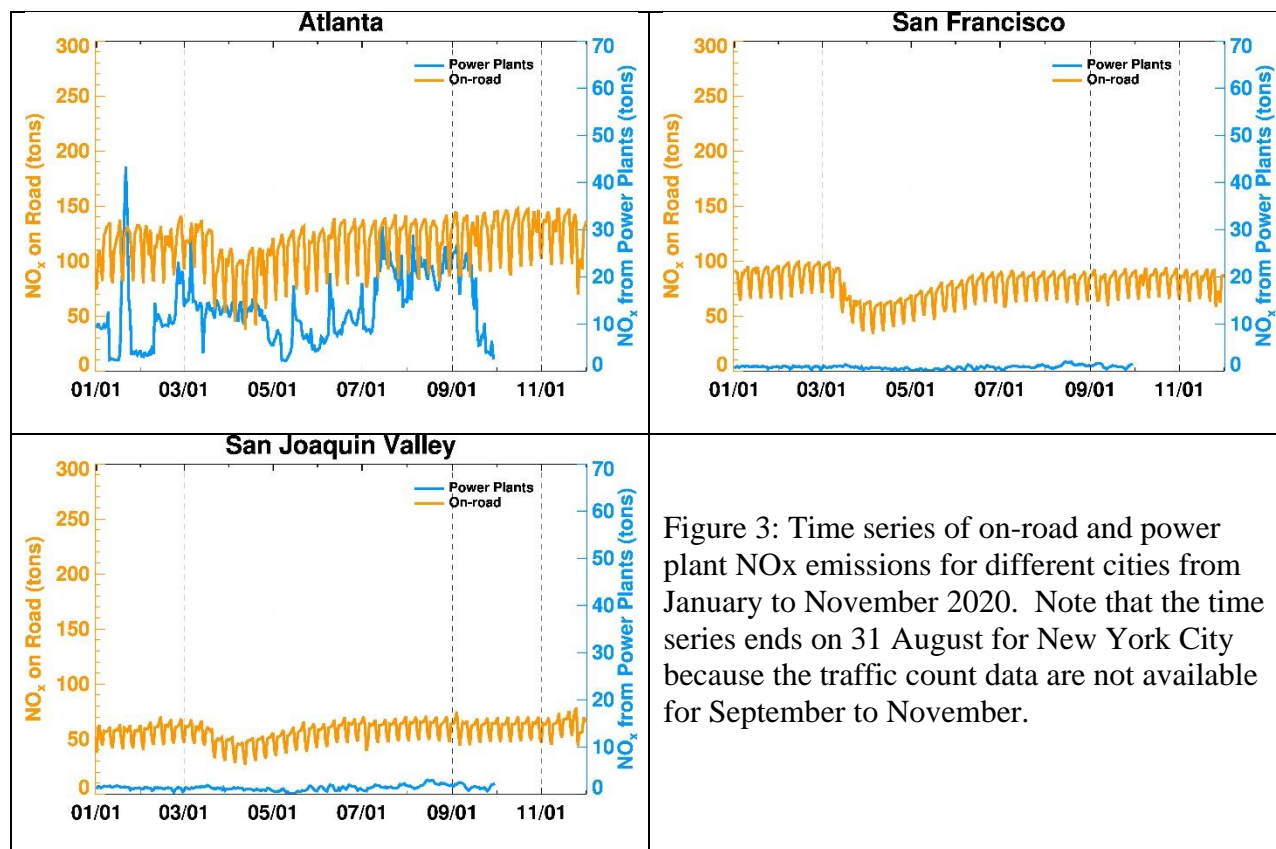
756

757

758

759
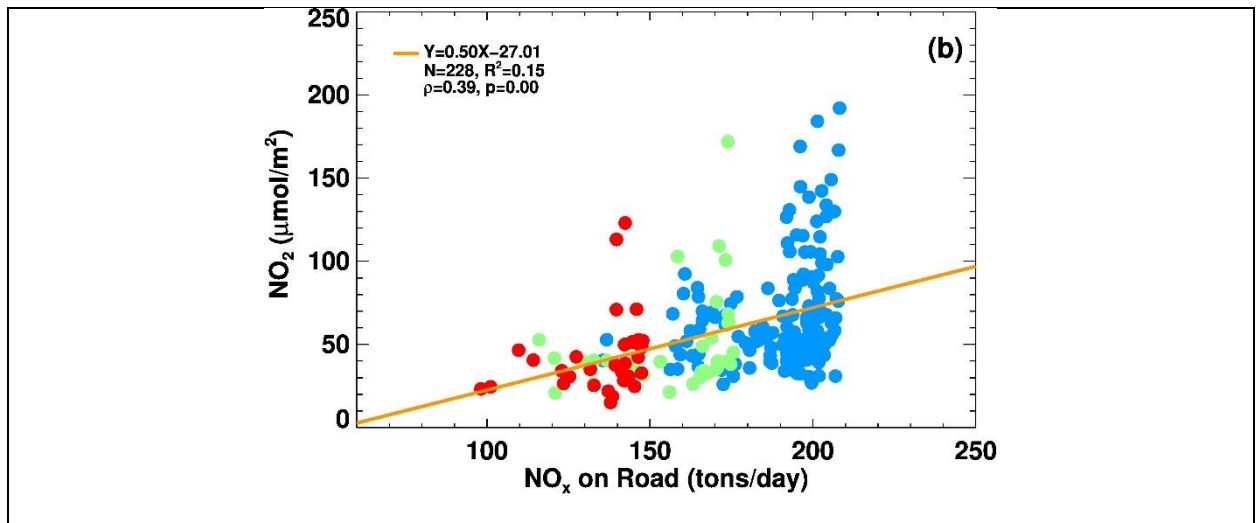
Figure 4: Correlation between tropNO$_2$ and on-road NO$_x$ emissions for Los Angeles, CA. (a) For pre-lockdown (January and February) and (b) For lockdown and post lockdown time period (March through end of November). Red color is for data gathered on Sundays, green color is for data gathered on Saturdays, and blue color is for data gathered on weekdays.
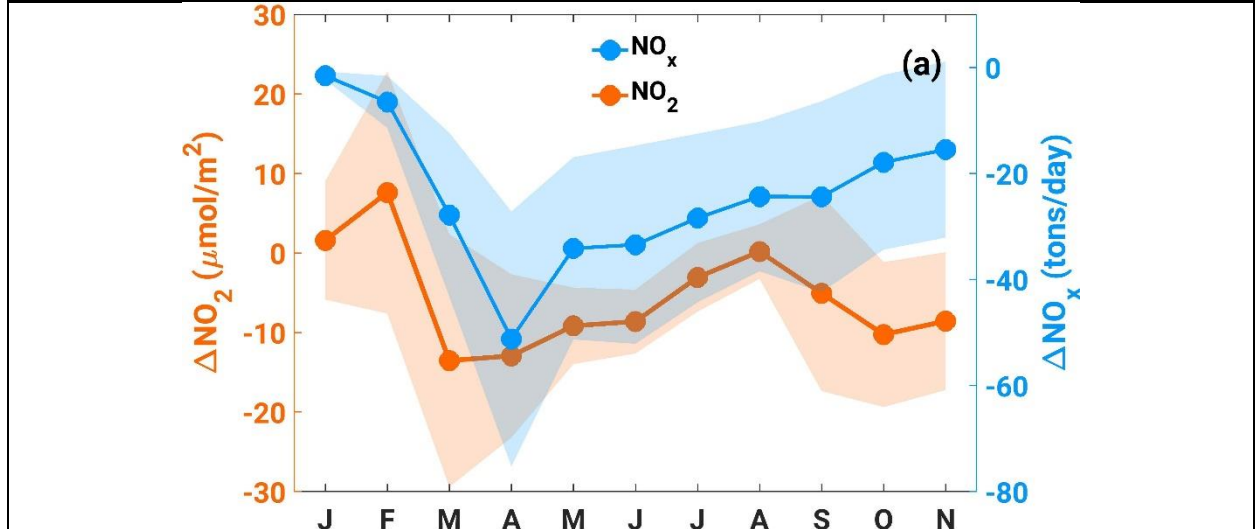
760

761

762

763

764

765

39
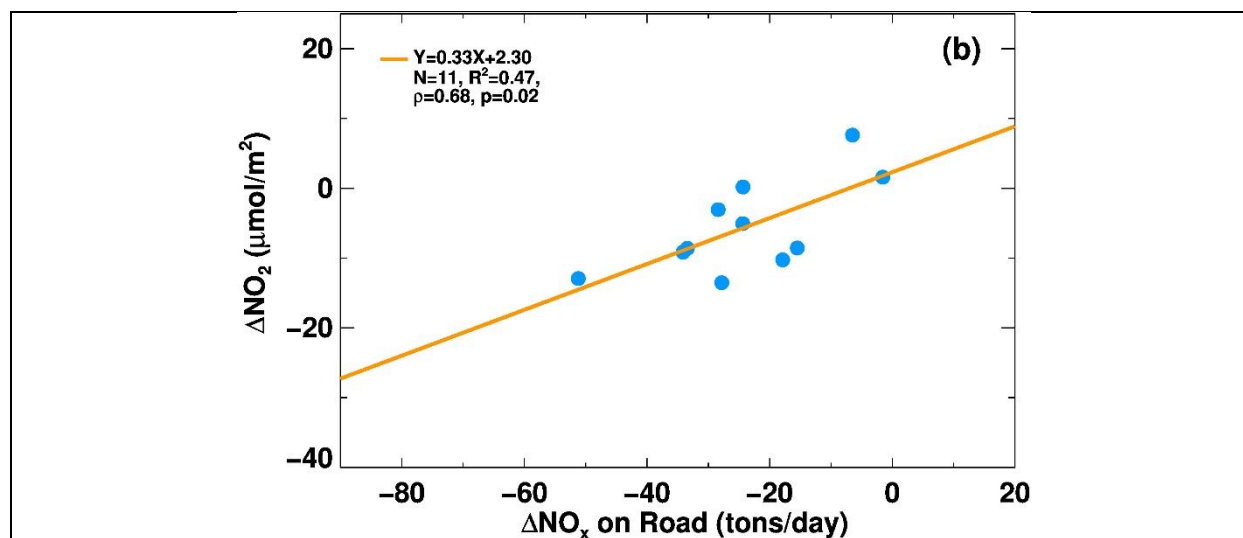
Figure 5: Trends in changes in on-road monthly mean NOx emissions (tons/day) and tropNO$_2$ (μmoles/m^2) between 2019 and 2020. (a) Average monthly mean differences for five cities (New York, Atlanta, Los Angeles, San Francisco, and San Joaquin Valley) across the United States from January to November. (b) Correlation between changes in on-road monthly mean NOx emissions and changes in tropNO$_2$ for the same five cities.

766

767

768

769

770

771

772

773
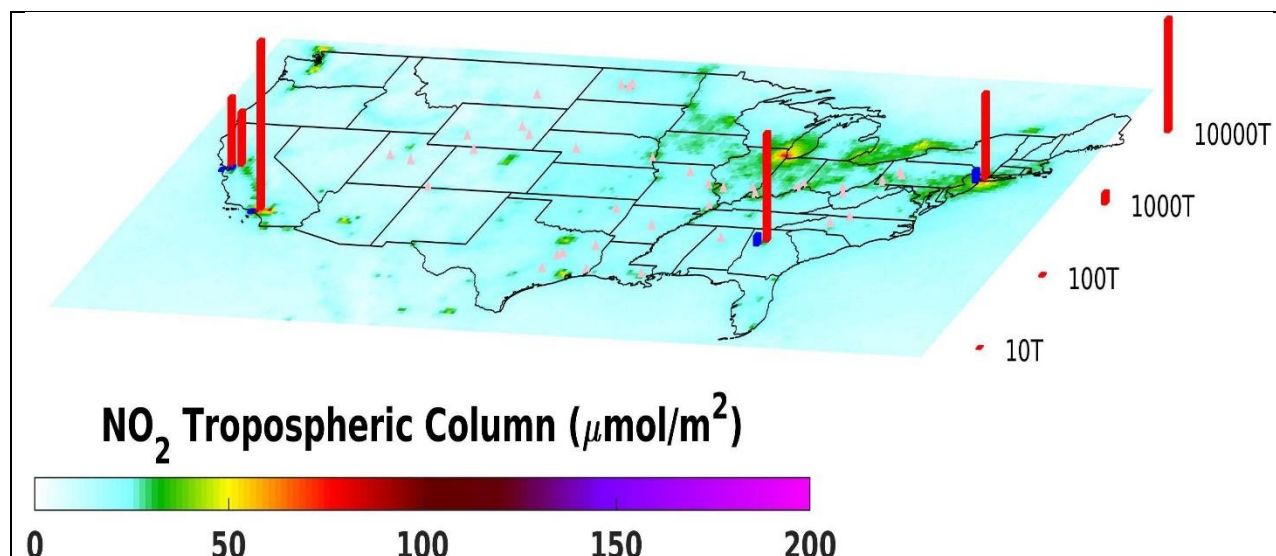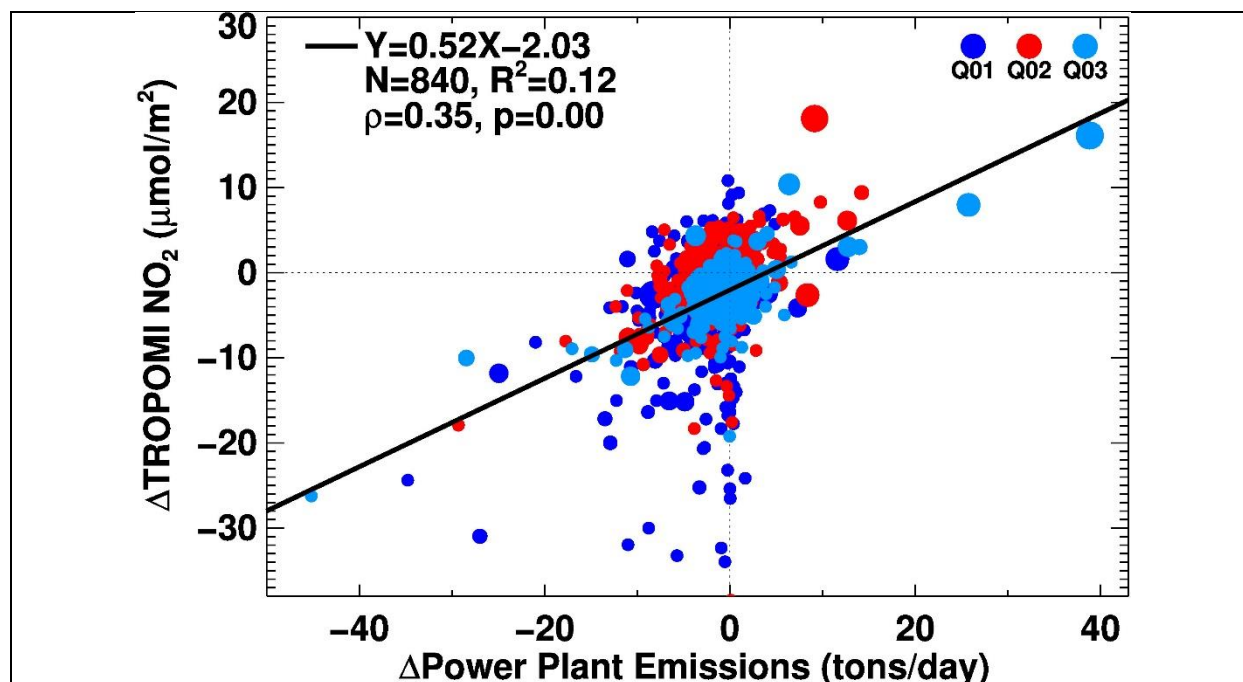
Figure 6: tropNO2 map for second quarter 2020 with the five locations where on-road NO_x emissions data were collected by NOAA. The red columns show total NOx emissions and the blue columns show NOx emissions from power plants nearby these five cities (New York, Atlanta, Los Angeles, San Francisco, and San Joaquin Valley). Power plants with monthly mean NOx emissions greater than 500 tons are also shown in the map as pink dots.

774

775

776

777

Figure 7: Correlation of tropNO$_2$ changes between 2020 and 2019 with changes in power plant monthly mean NO$_x$ emissions. Daily total NO$_x$ emissions were added and divided by the number of days in a month to get average values in units of tons/day.
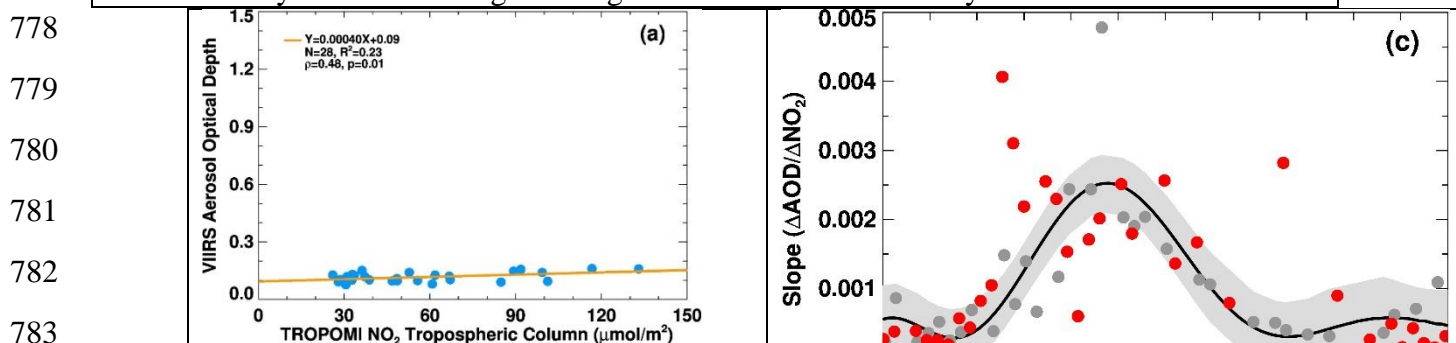
778

779

780

781

782

783

784

785

786

787

788

789

790

791

792

793

794

795

796

797

798

799

800

801

802

803
804
805
806
807
808

809
810
811
812
813
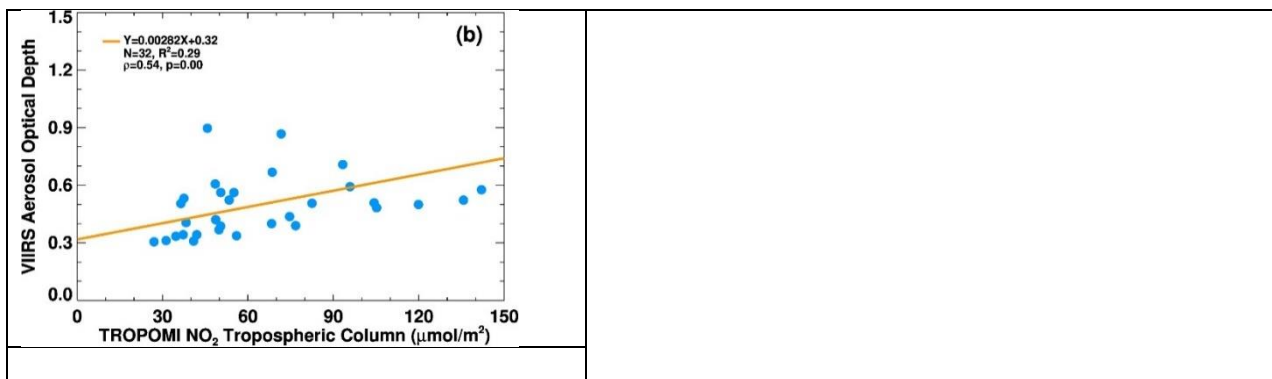
Figure 8: (a) Example correlation of VIIRS AOD and TROPOMI tropNO$_2$ during one week, September 15-21, 2019, (b) Same for September 13-19, 2020, (c) Time series of weekly slope (AOD/NO$_2$) with data for 2019 in gray color and data for 2020 in red color for Los Angeles, California. The black solid line is the fit to 2019 data indicating the photochemical processes of the impact of NOx on secondary aerosol formation. Any data points that depart from the fit line are treated as the time period when transported aerosols (e.g., smoke) influenced the air mass over Los Angeles.

814
815
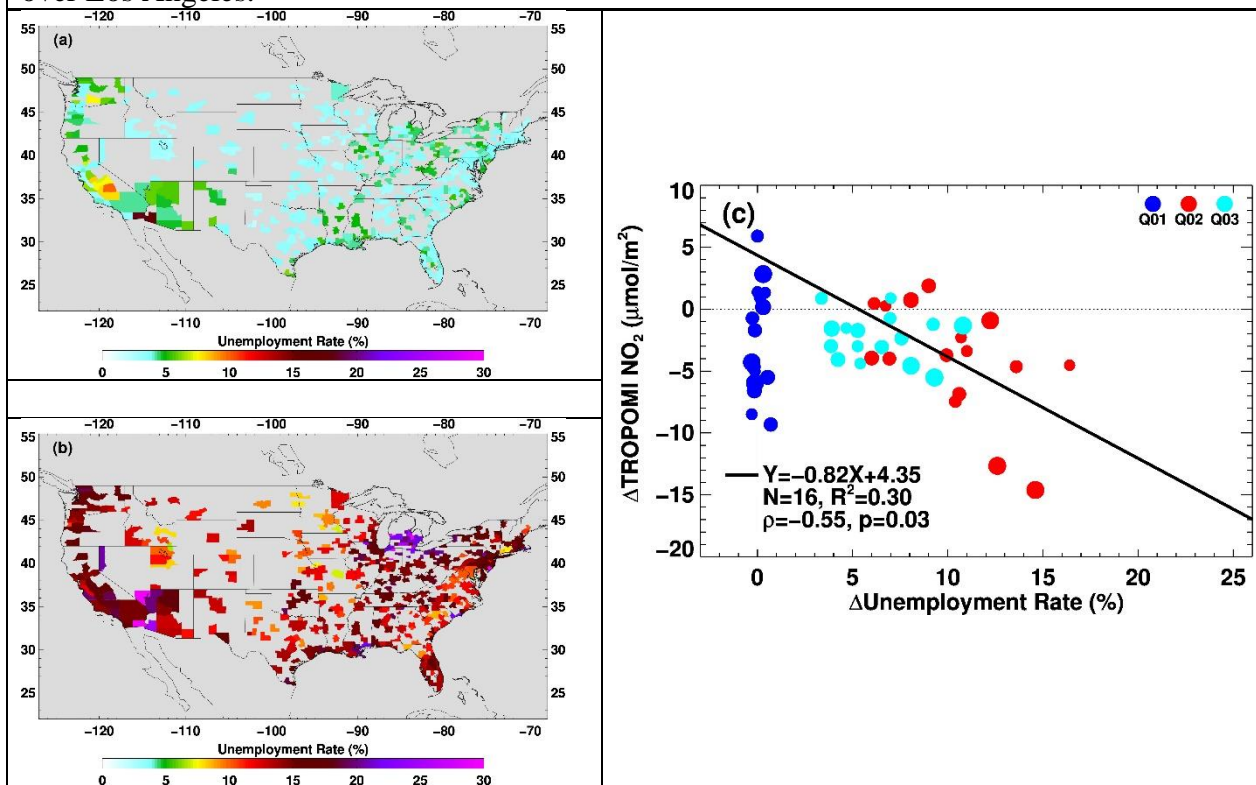
Figure 9: The impact of COVID-19 lockdown on unemployment rate in metropolitan areas and tropNO$_2$. (a) Unemployment rate in April 2019, (b) Unemployment rate in April 2020, and (c) Correlation between increase in unemployment between 2020 and 2019 and tropNO$_2$ changes. Only data for metropolitan areas where civilian labor force in 2019 was greater than two million

816
817
are shown in the correlation plot. In the first quarter (Q01) unemployment changes are close to zero as pandemic impact did not begin until late March. Strong negative correlation is observed for the second (Q02) and third (Q03) quarters. The solid black line is the fit to the second quarter data.

818

819

820

Table 1: Ranking of cities for ozone pollution and their lockdown time periods

821

822

823

824

825

826

827

828

829

830

831

832

833

834

835

836

837

838

839

840

841

842

843

City/Region	Ozone Pollution Ranking	Lockdown Start Date	Lockdown End Date
Los Angeles-Long Beach, CA	1	19-Mar	4-May
Visalia, CA	2	19-Mar	4-May
Bakersfield, CA	3	19-Mar	4-May
Fresno-Madera-Hanford, CA	4	19-Mar	4-May
Sacramento-Roseville, CA	5	19-Mar	4-May
San Diego-Chula Vista-Carlsbad, CA	6	19-Mar	4-May
Phoenix-Mesa, AZ	7	30-Mar	30-Apr
San Jose-San Francisco-Oakland, CA	8	19-Mar	4-May
Las Vegas-Henderson, NV	9	1-Apr	30-Apr
Denver-Aurora, CO	10	26-Mar	26-Apr
Salt Lake City-Provo-Orem, UT	11	30-Mar	13-Apr
New York-Newark, NY-NY-CT-PA*	12	22-Mar	15-May
Redding-Red Bluff, CA	13	19-Mar	4-May
Houston-The Woodlands, TX	14	2-Apr	20-Apr
El Centro, CA	15	19-Mar	4-May
Chicago-Naperville, IL-IN-WI*	16	23-Mar	1-May
El Paso-Las Cruces, TX-NM	17	2-Apr	15-May
Chico, CA	18	19-Mar	4-May
Fort Collins, CO	19	26-Mar	26-Apr
Washington-Baltimore-Arlington, DC-MD-VA-WV-PA*	20	30-Mar	15-May
Dallas-Fort Worth, TX-OK	21	2-Apr	20-Apr
Sheboygan, WI	22	24-Apr	26-May
Philadelphia-Reading-Camden, PA-NJ-DE-MD*	23	30-Mar	15-May
Milwaukee-Racine-Waukesha, WI	24	24-Apr	26-May
Hartford-East Hartford, CT	25	23-Mar	20-May

*Dates reflect the time period that is the longest for any given state in the region

844

845

846

847

848

849

850

851

852

853

854

855

856

857

858

859

860

861

862

863

864

865

866

867

868

869

870

871

872

873

Table 2: Reductions in on-road NOx emissions and tropNO2 between 15 March to 30 April and 1 January to 29 February						
City	2019ΔNOx (%)	2020ΔNOx (%)	Seasonality Removed On-road NOx Emissions Changes (%) 2020ΔNOx - 2019ΔNOx)	2019ΔNO2 (%)	2020ΔNO2 (%)	Seasonality Removed TropNO2 Reductions (%) (2020ΔtropNO$_2$ - 2019ΔtropNO$_2$)
Atlanta	10.41	-17.70	-28.11	-22.67	-44.14	-21.47
San Francisco	10.54	-33.95	-44.49	-23.79	-48.18	-24.39
San Joaquin Valley	14.27	-18.39	-32.66	-27.30	-44.62	-17.32
New York City	11.04	-36.87	-47,91	-6.07	-34.05	-27.98
Los Angeles	10.57	-25.10	-35.67	-37.90	-59.68	-21.78

874

875

876

877

878

879

880

881

882

883

884

885

886

887

888

889

890

891

References

Achakulwisut, P., Brauer, M., Hystad, P., Anenberg, S. C. (2019). Global, national, and urban burdens of paediatric asthma incidence attributable to ambient NO_2 pollution: estimates from global datasets. *Lancet Planet Health*. 1-4, DOI: 10.1016/S2542-5196(19)30046-4

Baidar, S., Hardesty, R. M., Kim, S.-W., Langford, A. O., Oetjen, H., Senff, C. J., et al. (2015).Weakening of the weekend ozone effect over California's South Coast Air Basin: Weekend ozone effect over California. *Geophysical Research Letters*, *42*, 9457–9464. doi: 10.1002/2015GL066419

Bauwens, M., Compernolle, S., Stavrakou, T., Muller, J.-F., van Gent, J., Eskes, H., Levelt, P. F., Van der A. R., Veefkind, P., Vlietinck, J., Yu, H., Zehner, C. (2020). *Geophysical Research Letters*. doi: 10.1029/2020GL087978

Bishop, G. A., and Stedman, D. H. (2014), The recession of 2008 and its impact on light-duty vehicle emissions in three western United States cities, *Environ Sci Technol*, *48*, 14822-14827, doi:10.1021/es5043518.

Bishop, G. A., and Haugen, M. J. (2018), The story of ever diminishing vehicle tailpipe emissions as observed in the Chicago, Illinois area, *Environ Sci Technol*, doi:10.1021/acs.est.8b00926.

Cersosimo, A., Serio, C., Masiello, G. (2020). TROPOMI NO_2 Tropospheric Column Data: Regridding to 1 km Grid-Resolution and Assessment of their Consistency with In Situ Surface Observations. *Remote Sens.*, *12*, 2212. https://doi.org/10.3390/rs12142212

Chan, K. L., M. Wiegner, J. van Geffen, I. De Smedt, C. Alberti, Z. Cheng, S. Ye, and M. Wenig, MAX-DOAS measurements of tropospheric NO2 and HCHO in Munich and the comparison to OMI and TROPOMI satellite observations (2020). *Atmos. Meas. Tech., 13*, 4499–4520. https://doi.org/10.5194/amt-13-4499-2020

de Gouw, J.A., Parrish, D.D., Frost, G.J. and Trainer, M. (2014), Reduced emissions of CO_2, NOx, and SO_2 from U.S. power plants owing to switch from coal to natural gas with combined cycle technology. Earth's Future, 2: 75-82. https://doi.org/10.1002/2013EF000196

EPA (2015), MOVES2014a (Motor Vehicle Emission Simulator), Office of Transportation and Air Quality, U.S. Environmental Protection Agency.

Fioletov, V. E., McLinden, C. A., Krotkov, N., Li, C. (2015). Lifetimes and emissions of SO2 from point sources estimated from OMI. *Geophys. Res. Lett*., *42*, 1969–1976, doi: 10.1002/2015GL063148.

935 Gkatzelis, G.I., J.B. Gilman, S.S. Brown, H. Eskes, A.R. Gomes, A.C. Lange, B.C. McDonald, J.
936 Peischl, A. Petzold, C. Thompson, A. Kiendler-Scharr (accepted). The Global Impacts of
937 COVID-19 Lockdowns on Urban Air Pollution: A Review. *Elementa: Science of Anthropocene*.
938
939 Goldberg, D. L., Anenberg, S. C., Griffin, D., McLinden, C. A., Lu, Z., & Streets, D.
940 G. (2020). Disentangling the impact of the COVID-19 lockdowns on urban NO_2 from natural
941 variability. *Geophysical Research Letters*, 47,
942 e2020GL089269. https://doi.org/10.1029/2020GL089269
943
944 Goldberg, D. L., Lu, Z., Streets, D. G., de Foy, B., Griffin, D., McLinden, C. A., Lamsal, L. N.,
945 Krotkov, N. A., Eskes, H. Enhanced capabilities of TROPOMI NO_2: Estimating NO_X from
946 North American 2 cities and power plants. (2019). *Environ. Sci. Technol.*, 53, 21, 12594–12601
947 https://doi.org/10.1021/acs.est.9b04488
948
949 Hassler, B., B. C. McDonald, G. J. Frost, A. Borbon, D. C. Carslaw, K. Civerolo, C. Granier, P.
950 S. Monks, S. Monks, D. D. Parrish, I. B. Pollack, K. H. Rosenlof, T. B. Ryerson, E. von
951 Schneidemesser, and M. Trainer (2016), Analysis of long-term observations of NOx and CO in
952 megacities and application to constraining emissions inventories, *Geophys Res Lett*, *43*, 9920-
953 9930, doi:10.1002/2016gl069894.
954
955 Hersbach, H, Bell, B, Berrisford, P, et al. The ERA5 global reanalysis. *Q J R Meteorol*
956 *Soc*. 2020; 146: 1999– 2049. https://doi.org/10.1002/qj.3803
957
958 Hoesly, R. M., Smith, S. J., Feng, L., Klimont, Z., Janssens-Maenhout, G., Pitkanen, T., Seibert,
959 J. J., Vu, L., Andres, R. J., Bolt, R. M., Bond, T. C., Dawidowski, L., Kholod, N., Kurokawa, J.-
960 I., Li, M., Liu, L., Lu, Z., Moura, M. C. P., O'Rourke, P. R., and Zhang, Q. (2018). Historical
961 (1750–2014) anthropogenic emissions of reactive gases and aerosols from the Community
962 Emissions Data System (CEDS). *Geosci. Model Dev.*, 11, 369–408.
963 https://doi.org/10.5194/gmd-11-369-2018
964 Huang, M., et al. (2014), Changes in nitrogen oxides emissions in California during 2005–2010
965 indicated from top-down and bottom-up emission estimates, *J. Geophys. Res.*
966 *Atmos.*, 119, 12,928– 12,952, doi:10.1002/2014JD022268.
967 Iolango, I., Virta, H., Eskes, H., Hovila, J., Douros, J. (2020). Comparison of
968 TROPOMI/Sentinel 5 Precursor NO_2 observations with ground-based measurements in Helsinki,
969 *Atmos. Meas. Tech.*, *13*, 205–218, https://doi.org/10.5194/amt-2019-329
970 Jiang, Z., B. C. McDonald, H. Worden, J. R. Worden, K. Miyazaki, Z. Qu, D. K. Henze, D. B. A.
971 Jones, A. F. Arellano, E. V. Fischer, L. Y. Zhu, and K. F. Boersma (2018), Unexpected
972 slowdown of US pollutant emission reduction in the past decade, *P Natl Acad Sci USA*, *115*,
973 5099-5104, doi:10.1073/pnas.1801191115.
974

975 Judd, L. M., J. A. All-Saadi, S. J. Janz, M. G. Kowalewski, R. B. Pierce, J. J. Szykman, L. C.
976 Valin, R. Swap, A. Cede, M. Mueller, M. Tiefengarber, N. Abuhassan, D. Williams, Evaluating
977 the impact of spatial resolution on tropospheric NO_2 column comparisons within urban areas
978 using high-resolution airborne data, https://doi.org/10.5194/amt-2019-161

979

980 Judd, L. M., Al-Saadi, J. A., Szykman, J. J., Valin, L. C., Janz, S. J., Kowalewski, M. G., Eskes,
981 H. J., Veefkind, J. P., Cede, A., Mueller, M., Gebetsberger, M., Swap, R., Pierce, R. B., Nowlan,
982 C. R., Abad, G. G., Nehrir, A., and Williams, D. (2020). Evaluating Sentinel-5P TROPOMI
983 tropospheric NO_2 column densities with airborne and Pandora spectrometers near New York
984 City and Long Island Sound, Atmos. Meas. Tech., 13, 6113–6140, https://doi.org/10.5194/amt-
985 13-6113-2020

986 Keller, C. A., Evans, M. J., Knowland, K. E., Hasenkopf, C. A., Modekurty, S., Lucchesi, R. A.,
987 Oda, T., Franca, B. B., Mandarino, F. C., Díaz Suárez, M. V., Ryan, R. G., Fakes, L. H., and
988 Pawson, S. (2020). Global Impact of COVID-19 Restrictions on the Surface Concentrations of
989 Nitrogen Dioxide and Ozone, Atmos. Chem. Phys. Discuss. [preprint],
990 https://doi.org/10.5194/acp-2020-685, in review.
991
992 Kim, S.-W., McDonald, B. C., Baidar, S., Brown, S. S., Dube, B., Ferrare, R. A., Frost, G.
993 J., Harley, R. A., Holloway, J. S., Lee, H.-J., et al. (2016), Modeling the weekly cycle of
994 NO_x and CO emissions and their impacts on O_3 in the Los Angeles-South Coast Air Basin during
995 the CalNex 2010 field campaign, *J. Geophys. Res. Atmos.*, 121, 1340– 1360,
996 doi:10.1002/2015JD024292.
997
998 Kondragunta, S., D. Crisp, and C. Zehner (2020), Disseminating scientific results in the age of
999 rapid communication, *Eos, 101,* https://doi.org/10.1029/2020EO150710. Published on 20
1000 October 2020.

1001
1002 Kroll, J.H., Heald, C.L., Cappa, C.D. *et al.* The complex chemical effects of COVID-19
1003 shutdowns on air quality. *Nat. Chem.* **12,** 777–779 (2020). https://doi.org/10.1038/s41557-020-
1004 0535-z
1005

1006 Lamsal, N. L., Duncan, B.N., Yoshida, Y., Krotkov, N. A., Pickering, K. E., Streets, D. (2015).
1007 U.S. NO_2 trends (2005–2013): EPA Air Quality System (AQS) data versus improved
1008 observations from the Ozone Monitoring Instrument (OMI), *Atmospheric Environment*, *100,*
1009 130-143.

1010 Laszlo, I. and Liu, H., 2016. EPS Aerosol Optical Depth (AOD) Algorithm Theoretical Basis
1011 Document, version 3.0.1, June 28, 2016, NOAA NESDIS.
1012

1013 Levy, R.C., Remer, L.A., Mattoo, S., Vermote, E.F., and Kaufman, Y.J. (2007). Second-
1014 generation operational algorithm: retrieval of aerosol properties over land from inversion of

1015 Moderate Resolution Imaging Spectroradiometer spectral reflectance. *J Geophys Res*., *112*.
1016 doi:10.1029/2006JD007811

1017

1018 Lin, J.-T., Martin, R. V., Boersma, K. F., Sneep, M., Stammes, P., Spurr, R., Wang, P., Van
1019 Roozendael, M., Clémer, K., and Irie, H. (2014). Retrieving tropospheric nitrogen dioxide from
1020 the Ozone Monitoring Instrument: effects of aerosols, surface reflectance anisotropy, and vertical
1021 profile of nitrogen dioxide, *Atmos. Chem. Phys., 14*, 1441–1461. https://doi.org/10.5194/acp-14-
1022 1441-2014

1023 Liu, F., Page, A., Strode, S. A., Yoshida, Y., Choi, S., Zheng, B., Lamsal, L., Li, C., Krotkov, N.
1024 A., Eskes, H., van der, R., Veefkind, P., Levelt, P. F., Hauser, O. P., Joiner, J. (2020). Abrupt
1025 decline in tropospheric nitrogen dioxide over China after the outbreak of COVID-19, *Science
1026 Advances, 6*, 28, eabc2992. DOI: 10.1126/sciadv.abc2992

1027 Liu, M., J. Lin, H. Kong, K. F. Boersma, H. Eskes, Y. Kanaya, Q. Hes, X. Tian, K. Qin, P. Xie,
1028 R. Spurr, R. Ni, Y. Yan, H. Weng, J. Wang (2020). A new TROPOMI product for tropospheric
1029 NO_2 columns over East Asia with explicit aerosol corrections. *Atmos. Meas. Tech., 13*, 4247–
1030 4259. https://doi.org/10.5194/amt-13-4247-2020

1031 Lorente, A., Boersma, K.F., Eskes, H.J. *et al.* Quantification of nitrogen oxides emissions from
1032 build-up of pollution over Paris with TROPOMI. *Sci Rep* **9,** 20033 (2019).
1033 https://doi.org/10.1038/s41598-019-56428-5

1034 Mazuuca, G. M., X. Ren, C. P. Loughner, M. Estes, J. H. Crawford, K. E. Pickering, A. J.
1035 Weinheimer, and R. R. Dickerson, Ozone production and its sensitivity to NOx and VOCs:
1036 results from the DISCOVER-AQ field experiment, Houston 2013. 2016. *Atmos. Chem. Phys.,
1037 16,* 14463–14474. doi: 10.5194/acp-16-14463-2016

1038 McDonald, B. C., S. A. McKeen, Y. Y. Cui, R. Ahmadov, S. W. Kim, G. J. Frost, I. B. Pollack,
1039 T. B. Ryerson, J. S. Holloway, M. Graus, C. Warneke, J. B. Gilman, J. A. de Gouw, J. Kaiser, F.
1040 N. Keutsch, T. F. Hanisco, G. M. Wolfe, and M. Trainer (2018), Modeling ozone in the Eastern
1041 U.S. using a fuel-based mobile source emissions inventory, *Environ Sci Technol*, *52*, 7360-7370,
1042 doi:10.1021/acs.est.8b00778.

1043 McDonald, B. C., T. R. Dallmann, E. W. Martin, and R. A. Harley (2012), Long-term trends in
1044 nitrogen oxide emissions from motor vehicles at national, state, and air basin scales, *J Geophys
1045 Res-Atmos*, *117*, D00V18, doi:10.1029/2012jd018304.

1046

1047 McDonald, B. C., Z. C. McBride, E. W. Martin, and R. A. Harley (2014), High-resolution
1048 mapping of motor vehicle carbon dioxide emissions, *J Geophys Res-Atmos*, *119*, 5283-5298,
1049 doi:10.1002/2013jd021219.

1050 McDonald, B. C., Dallmann, T. R., Martin, E. W., and Harley, R. A. (2012), Long-term trends in
1051 nitrogen oxide emissions from motor vehicles at national, state, and air basin scales, *J. Geophys.
1052 Res.*, 117, D00V18, doi: 10.1029/2012JD018304

1053   McDonald, B. C., et al. (2018). Volatile chemical products emerging as largest petrochemical
1054   source of urban organic emissions. *Science 359*, 760-764.

1055   Naeger, A.R. and Murphy, K. (2020). Impact of COVID-19 Containment Measures on Air
1056   Pollution in California. *Aerosol Air Qual. Res.* https://doi.org/10.4209/aaqr.2020.05.0227

1057   Parker, H. A., Hasheminassab, S., Crounse, J. D., Roehl, C. M., & Wennberg, P. O. (2020).
1058   Impacts of traffic reductions associated with COVID-19 on Southern California air quality.
1059   Geophysical Research Letters, 47, e2020GL090164. https://doi.org/10.1029/2020GL090164
1060

1061   Qin, M., Murphy, B.N., Isaacs, K.K. *et al.* (2021). Criteria pollutant impacts of volatile chemical
1062   products informed by near-field modelling. *Nat Sustain 4***,** 129–137.
1063   https://doi.org/10.1038/s41893-020-00614-1

1064   Silver, B., X. He, S. Arnold, D. V. Spracklen, The impact of COVID-19 control measures on air
1065   quality in China. (2020). *Environ. Res. Lett. 15*, 084021. https://doi.org/10.1088/1748-
1066   9326/aba3a2

1067   Schiferl, L. D., C. L. Heald, J. B. Nowak, J. S. Holloway, J. A. Neuman, R. Bahreini, I. B.
1068   Pollack, T. B. Ryerson, C. Wiedinmyer, and J. G. Murphy (2014), An investigation of ammonia
1069   and inorganic particulate matter in California during the CalNex campaign, J. Geophys. Res.
1070   Atmos., 119, 1883–1902, doi:10.1002/2013JD020765

1071   Silvern, R. F., D. J. Jacob, L. J. Mickley, M. P. Sulprizio, K. R. Travis, E. A. Marais, R. C.
1072   Cohen, J. L. Laughner, S. Choi, J. Joiner, and L. N. Lamsal, Using satellite observations of
1073   tropospheric NO_2 columns to infer long-term trends in US NOx emissions: the importance of
1074   accounting for the free tropospheric NO_2 background. (2019). *Atmos. Chem. Phys., 19*, 8863–
1075   8878. https://doi.org/10.5194/acp-19-8863-2019

1076   Tack, F., A. Merlaud, A. C. Meir, T. Vlemmix, T. Ruhtz, M-D. Iordache, X. Ge, :/ vam der War.
1077   D/ Schuettemeyer, M. Ardelean, A. Calcan, D. Constantin, A. Schonhardt, K. Meuleman, A.
1078   Richter, and M. V. Roozendae, Intercomparison of four airborne imaging DOAS systems for
1079   tropospheric NO_2 mapping – the AROMAPEX campaign. (2019). *Atmos. Meas. Tech.,12*, 211–
1080   236. https://doi.org/10.5194/amt-12-211

1081   Today in energy, https://www.eia.gov/todayinenergy/detail.php?id=37752, December 11, 2018

1082   Tong, D., L. Pan, W. Chen, L. Lamsal, P. Lee, Y. Tang, H. Kim, S. Kondragunta, I. Stajner,
1083   Impact of the 2008 Global Recession on air quality over the United States: Implications for
1084   surface ozone levels from changes in NOx emissions. (2016). *Geophys. Res. Lett.,*
1085   *10*.1002/2016GL069885

1086   Tong, D.Q., L. Lamsal, L. Pan, C. Ding, H. Kim, P. Lee, T. Chai, and K.E. Pickering, and I.
1087   Stajner, Long-term NOx trends over large cities in the United States during the 2008 Recession:
1088   Intercomparison of satellite retrievals, ground observations, and emission inventories. (2015).
1089   *Atmospheric Environment, 107*, 70-84. doi:10.1016/j.atmosenv.2015.01.035

1090
1091 van Geffen, J., H. J. Eskes, K. F. Boresma, J. D. Maasakkers, and J. P. Veefkind, TROPOMI
1092 ATBD of the total and tropospheric NO_2 data products, S5P-KNMI-L2-0005-RP, v1.4.0, 2019

1093 Zhang, Q., Y. Pan, Y. He, W. W. Walters, Q. Ni, X. Liu, G. Xu, J. Shao, C. Jiang, Substantial
1094 nitrogen oxides emission reduction from China due to COVID-19 and its impact on surface
1095 ozone and aerosol pollution. (2021). *Science of The Total Environment, 753*.

1096 Zhao, X., D. Griffin, V. Fioletov, C. McLinden, A. Cede, M. Tiefengraber, M. Muller, K.
1097 Bognar, K. Strong, F. Boersma, H. Eskes, J. Davies, A. Ogyu, and S. C. Lee. (2020).
1098 Assessment of the quality of TROPOMI high-spatial-resolution NO_2 data products in the Greater
1099 Toronto Area, *Atmos. Meas. Tech., 13*, 2131–2159. https://doi.org/10.5194/amt-13-2131-2020

1100 Zhang, H., & Kondragunta, S. (2021). Daily and Hourly Surface PM2.5 Estimation from
1101 Satellite AOD. *Earth and Space Science*, 8,
1102 e2020EA001599. https://doi.org/10.1029/2020EA001599

1103 Zheng, H., S. Kong, N. Chen, Y. Yan, D. Liu, B. Zhu, K. Xu, W. Cao, Q. Ding, B. Lan, Z.
1104 Zhang, M. Zheng, Z. Fan, Y. Cheng, S. Zheng, L. Yao, Y. Bai, T. Zhao, S. Qi. (2020).
1105 Significant changes in the chemical compositions and sources of PM2.5 in Wuhan since the city
1106 lockdown as COVID-19, Science of the Total Environment, 739.

1107
1108